ERASMUS UNIVERSITY ROTTERDAM
ERASMUS SCHOOL OF ECONOMICS
Master Thesis Quantitative Finance

# Beyond the Breaking Point: Assessing the Financial Consequences of Climate Tipping Points

Joris Knoester (479288)


| | |
|---|---|
| Supervisor: | Wendun Wang |
| Second assessor: | Philip Hans Franses |
| Date final version: | July 13, 2023 |

**Abstract**

As global warming continues to degrade the Earth, the need to understand and mitigate the impact of climate change has become increasingly urgent. Temperatures are rising, increasing the chance of activating climate mechanisms, known as climate tipping points, which have the potential to critically alter the world. To assess their impact on economic growth, the ADICT+MSL model breaks down the climate tipping points into three distinct elements: activation, damage, and interaction, while accounting for rising sea levels. The study reveals the consequences of climate change. Rising sea levels emerge as the key determinant of climate tipping point danger. Whereas the baseline model projects annual gross domestic product growth rates of 3.3%, 2.4%, and -0.4% in 2122 for the Representative Concentration Pathways 2.6, 4.5, and 8.5, respectively, the additional relative damage from climate tipping points is 0.9, 1.0, and 3.0 percentage. Furthermore, it is alarming that the depreciation in economic growth is most pronounced in less developed regions. In terms of financial indicators, significant drops in stock market returns, inflation, and long-term interest rates are anticipated. In conclusion, immediate actions to diminish global warming and prevent climate tipping points activation is imperative to avert severe economic disruptions.

# Chapter 1

# Introduction

Former American President Barack Obama once said: "We are the first generation to feel the impact of climate change and the last generation that can do something about it." Earth's climate has deteriorated due to greenhouse gas emissions, with the current global temperature anomaly at approximately $+1.25°$C compared to the 1850-1900 average (Rohde, 2023). In the winter of 2023, several European countries experienced record-breaking high temperatures, including a $20.2°$C measurement in the Alps, representing a sixteen degree increase compared to the past 30-year average (Meredith, 2023).

According to a study by Carnegie Mellon University, under the Paris Agreement's target of limiting temperature rise to +1.5°C, 49% of ice caps could melt by 2100, while a temperature anomaly of +4.0°C could result in the disappearance of 83% of glaciers. The Paris Agreement, signed by 196 countries, aims to prevent global warming from exceeding certain thresholds. However, current projections indicate a temperature rise of +2.7°C by the end of the century. This excessive temperature is particularly distressing because +1.5°C equals the temperature level at which the first Climate Tipping Points (CTPs) may start to occur. CTPs are irreversible, geological mechanisms that can have catastrophic consequences on a global scale. Herr, Osaka, and Stone (2019) and Igini (2022) describe the nature and danger of CTPs in their research.

Carrington (2022b) and Hersher and Sommer (2022) illustrate the likelihood of multiple CTPs to change states within the next 100 years. One hazardous example of a CTP that is probable to happen in the near future is the melting of the Greenland Ice Sheet (GIS). This would increase the global mean sea level substantially, leading to massive population migrations, which local governments could not manage. Preventing these events should be the primary focus to avoid irreversible damage.

The sole weapon that can change current collapse of the climate is cooperative global politics. For instance, the Montreal Protocol of 1987 has recently demonstrated its effectiveness in restoring the Earth's protective ozone layer. Newburger (2023) projects that the ozone hole recovers within four decades after its detection in 1980. Despite consensus that global warming is a dangerous dy-

namic that needs to be stopped, politics are often only executed, motivated by financial incentives. To provide an economic stimulus, this paper combines expert climate literature with modern econometric techniques to estimate the impact of CTPs on Gross Domestic Product (GDP) growth rates and financial variables. The research demonstrates a simulation over the next 100 years, 2023-2122. Subsequently, this study aims to answer the following main research question:

*What is the expected effect of climate tipping points on GDP growth rates for the next 100 years?*

It is scientifically accepted that temperature causes the tipping of climate mechanisms, thereby reducing global GDP growth (Dietz, Rising, Stoerk, & Wagner, 2021) (McKay et al., 2022) (Rebonato, Kainth, & Melin, 2022). However, there exists considerable uncertainty regarding the magnitude of temperature change in the future. Therefore, this paper examines the influence of different temperature tracks, as presented in the Representative Concentration Pathways (RCP) datasets, introduced by Meinshausen et al. (2011) and presented in the Intergovernmental Panel on Climate Change (IPCC) 2014 annual report (IPCC, 2014). Additionally, the impact of mean sea level rise due to CTPs that contain substantial amounts of water is explored. Hence, the first two sub-questions are:

*What is the expected impact of CTPs on GDP growth rates for different temperature pathways?*

*What is the expected impact of CTP-induced sea level rise on GDP growth rates?*

Also, the properties of individual CTPs are ambiguous. To address this, a sensitivity analysis on three aspects is conducted. First, the tipping probability is scrutinized. Next, because McKay et al. (2022) and Rocha, Peterson, Bodin, and Levin (2018) argue that CTPs are likely to happen consecutively, the influence of an increased probability of a cascade effect in the CTPs is examined. Third, the effect of the mean sea level damage is evaluated. This leads to the final two sub-questions:

*How does the tipping probability affect the expected impact of climate tipping points on GDP growth rates for the next 100 years?*

*How does the probability of cascading regime shifts affect the expected impact of climate tipping points on GDP growth rates for the next 100 years?*

This paper introduces a mathematical network, Activation and Damage of Interactional Climate Tipping Points (ADICT), that incorporates the effects of Climate Tipping Points (CTPs) using IPCC RCP 2.6, 4.5, and 8.5 datasets. The ADICT model focuses on the activation and external damage of individual CTPs, with an additional mean sea level (MSL) module to estimate the increase in mean sea level, drawing on research by Aschwanden et al. (2019), Bulthuis, Arnst, Sun, and Pattyn (2019), Fretwell et al. (2013), Marzeion, Kaser, Maussion, and Champollion (2018), Pan et al. (2021), and Rignot and Thomas (2002). This approach is designed to be simple, making it applicable to

multiple CTPs, and interpretable for a broad audience in the political and financial business as well as environmental scientists. The goal of this study is to inform this group of people about the negative consequences of climate change by analyzing the impact of global warming with respect to GDP growth and economic indicators. The economic variables are equity returns, inflation rates, long-term interest rates, and unemployment rates.

To the best of our knowledge, no existing model estimates the economic effects of multiple CTPs while considering their interaction. Additionally, the influence of mean sea level on financial variables is often overlooked. This paper addresses these gaps in the literature and contributes valuable insights.

Considering the short- and long-term effects of climate change, the impact of CTPs on GDP growth is expected to be a gradual long-term process, while economic indicators may reflect short-term shocks caused by extreme weather events. The damage to GDP can result from changes in agricultural productivity, infrastructure damage, and altered economic systems. In contrast, regional equity returns, inflation rates, long-term interest rates, and unemployment rates can be influenced by supply chain disruptions, crop failures, and job losses, leading to financial market shocks. To capture both types of effects, this research examines the cumulative 100-year GDP growth rate and analyzes selected critical CTP years to understand their impact on economic time series. The Python code is available through GitHub: https://github.com/jorisknoester/ADICT-MSL.

The findings indicate that CTPs diminish the expected global GDP growth rate, specifically due to the additional mean sea level impact. Whereas the sole temperature adjustment in ADICT does not produce significant differences compared to BASE, the weighted world GDP growth rate with ADICT+MSL in 2122 is 2.4%, 1.4%, and -3.4% for RCP2.6, RCP4.5, and RCP8.5, respectively. In perspective, BASE results in 3.3%, 2.4%, and -0.4%. The results are sensitive to the parameter value for the probability of tipping, $\tau$. As anticipated, a higher probability of tipping produces a lower GDP growth rate. On the other hand, the increased cascading effect does not influence the results substantially. Last, the Earth's warming damages the less developed countries the most significant, both in terms of GDP as the other financial assets that are examined. Overall, the inflation rates, long-term interest rates, and especially the stock market returns are expected to experience significant declines over time due to global warming and CTPs, leading to negative annual rates. On the other hand, the unemployment rates stays constant.

The paper is organized as follows: Chapter 2 provides a review of the literature on global warming modeling and CTPs. Chapter 3 explores the mathematical aspects of CTPs, the damage function, and the rationale for selecting financial variables. Chapters 4 and 5 describes the data and methods employed in the study. Chapter 6 presents the findings, which are discussed and summarized in Chapters 7 and 8.

# Chapter 2

# Literature review

This chapter provides an overview of the existing literature on climate change and CTPs. It is divided into four sections. The first section examines the use of Integrated Assessment Models (IAMs) in climate research. Section 2.2 analyzes papers that include a damage function and Section 2.3 describes existing models covering CTPs. The final section explores the relationship between CTPs and mean sea level.

## 2.1 Integrated Assessment Models

"Planet Earth is habitable because of its location relative to the sun and because of the natural greenhouse effect of its atmosphere" (Karl & Trenberth, 2003). Although it is impossible to alter the Earth's position, it is painful that human activities are currently degrading the greenhouse effect of the planet. Karl and Trenberth (2003) observed that, while total solar irradiance caused a 0.2°C temperature rise during the first half of the $20^{th}$ century, the human population have since dominated climate change. According to Wheeler and Von Braun (2013), global warming is likely to result in under-nutrition and starvation in regions that already suffer from hunger. While the world's population is still growing and demanding more wheat, food resources are becoming scarce. This negative diverging trend will have the most significant impact on the southern hemisphere.

Despite the importance of reporting, climate modeling is a complex process involving uncertainties, gaps in evidence, and the need for expert knowledge. To address these issues, IAMs were introduced to combine different climate models into a unified system. IAMs focus on areas, such as biodiversity, loss of life, and population migrations. They are a crucial link between human activities and global warming and are used as advisory tools for policy-making. Nordhaus (1992), Hope, Anderson, and Wenman (1993), and Rotmans, Hulme, and Downing (1994) developed commonly utilized climate models, such as DICE, PAGE, and ESCAPE, respectively.

Hansen and et al. (2005) were the first to present the existence of CTPs, which led to stochastic IAMs models to account for them. Lontzek, Cai, Judd, and Lenton (2015) introduced the DSICE model, which is a stochastic variant of the DICE. It contains a module that predicts the regime shifts of CTPs and suggests that the optimal carbon tax rate should increase by 50%. In addition, Dietz et al. (2021) assembled existing literature and combined the effects of multiple CTPs into one detailed cohesive structure. They created an IAM to estimate the change in temperature and mean sea level. Although their analysis is highly respected, the complexity of their approach and the difficulty of adapting and improving it remain major challenges. These are general challenges of IAMs Parson and Fisher-Vanden (1997). Other challenges include extensive expert knowledge, oversight of extreme events (Dowlatabadi, 1995) and overlooking time-dependent dynamics (Schwanitz, 2013).

## 2.2 Damage function models

In contrast to IAMs that generate a range of climate measures, other researchers focus on the impact of climate change on global economic growth, based on (non-linear) regressions on historical data (Kalkuhl & Wenz, 2020) (Kahn et al., 2021) (Burke & Tanutama, 2019). There are two types of physical climate risks, acute physical risks and chronic physical risks. The prior refers to event-driven damage, including extreme weather events, the second covers long-term adaptions in climate trends. In the remainder of this study and the provided papers, the long-horizon effect of chronic physical risks are examined. The study of Kalkuhl and Wenz (2020) breaks down the predicted GDP growth rate into three components; the immediate climate effect, the transitory effect, and the balanced growth path. They predict that, in the most severe scenario, temperature will increase by 2.88°C in 2099. The 2.88 temperature rise leads to a -11.4% impact on Gross Regional Product with the most significant impact on southern countries. Furthermore, Kahn et al. (2021) forecasted a 7.22% decrease in real GDP by 2100 if the temperature rises by 0.04°C per year. Unlike Kalkuhl and Wenz (2020), they consider the ratio of physical capital to effective units of labor inputs as an independent variable in the damage function. Finally, Burke and Tanutama (2019) develop a damage function that includes precipitation, as well as fixed country and year effects. They assemble geographical economic data for 11,000 districts and determine that the US and EU lost $4 trillion from 2000 until 2019 due to global warming. Similar to Kalkuhl and Wenz (2020), they argue that the impact is the most significant in the more southern regions. The economic contraction in these regions exceed 5% over the specified period.

## 2.3 Climate tipping point models

Two studies by Brammer, Lightwoord, and Rossi (2022) and Rebonato et al. (2022) examine the economic output damage function and the evaluation of CTPs in the context of climate change. First of all, Brammer et al. (2022) present an integrated model that incorporates both physical and transitional damage, considering physical damage as the primary driver of transitional risk. Their model combines a carbon threshold model, a mathematical integral with a marginal abatement curve, and a Poisson counter process to account for the effects of CTPs on financial assets. The findings indicate potential long-term decreases in the value of US mortgage-backed securities and equity assets due to global warming.

Rebonato et al. (2022), on the other hand, proposes a logistic damage function to quantify the external damage caused by CTPs. The model is designed to be simple and interpretable, relying on temperature and a damage parameter coefficient. The damage parameter is drawn from a logistic distribution to address uncertainty. Three government abatement schedules are estimated, with the *FAST* schedule showing superior performance, particularly in the tails of the distribution. The study emphasizes that CTPs amplify the effects of climate change.

However, both studies overlook the interaction between different CTPs and fail to account for the impacts of ocean levels. The paper of Rocha et al. (2018) emphasizes the significance of considering the interactions among CTPs and classifies them into three categories: *shared drivers*, *domino effects*, and *hidden feedbacks*. These relationships, retrieved using the Regime-Shifts Database (Biggs, Peterson, & Rocha, 2015), differ in the directional nature of the interactions. The authors stress that analyzing CTPs necessitates accounting for their interactions. Therefore, this study incorporates the relationships between individual CTPs through the ADICT module.

## 2.4 Mean sea level rise

In order to also incorporate the mean sea level change due to CTPs, the ADICT system is extended with the MSL module. According to a warning by Hanes (2022), the ice sheets in Antarctica have been declining at an accelerating rate over the past thirty years, with a sixfold increase in the rate of decline. The West Antarctic Ice Sheet (WAIS) has melted completely in the past for several times, indicating its sensitivity to global warming and its instability. The complete melting of the WAIS could contribute up to three meters of ocean level equivalence. Additionally, although the East Antarctic Ice Sheet (EAIS) is generally considered more stable, it has also shown signs of losing mass balance over the past two decades. It contains an equivalent of 60 meters of mean sea level. This highlights the need for caution regarding recent negative developments. Furthermore, Carrington (2022a) inves-

tigated the Greenland Ice Sheet (GIS) and claim that it will inevitably add 27 centimeters to ocean levels and this could increase to 78 centimeters within a few years, depending on future emissions levels. Surprisingly, Harvey (2019) states that the recent melting of glaciers accounts for one-third of mean sea level rise, surpassing the combined impact of the WAIS, EAIS, and GIS. Therefore, glaciers are a crucial component of climate change.

As shown, many scientists have investigated the direct impact of individual CTPs that include ice sheets on ocean level. The findings of the following studies are included in our model. Based on historical data from the Pliocene epoch, DeConto and Pollard (2016) estimated that the AIS alone could cause a 13-meter rise in ocean level by 2500. In response, Bulthuis et al. (2019) proposed a probabilistic approach that uses the f.ETISH model (Pattyn et al., 2017) to simulate the reaction of the AIS to environmental and parametric perturbations. In their model, an global ocean level rise of three centimeters is anticipated by 2100 and eight centimeters at the end of the horizon period in 2200 due to the AIS for the RCP2.6 scenarios. However, under the RCP8.5 emission path, this could increase to 11 centimeters and 45 centimeters, respectively. Furthermore, Pan et al. (2021) and Fretwell et al. (2013) have performed an extensive analysis of the ice sheet caps in both the EAIS and WAIS area and find that the possible increase in mean sea level due to a total collapse of both ice sheets is 53 meters and 4 meters, respectively. Regarding GIS, the study of Alley, Clark, Huybrechts, and Joughin (2005) predicts a mean sea level rise contribution of 0.5 mm/y on average. Again, this value is sensitive to the climate path used. In comparison, Aschwanden et al. (2019) utilized the PISM model (Winkelmann et al., 2011) to project an ocean level increase of five centimeters due to GIS for the RCP2.6 path and 33 centimeters by 2100 for the RCP8.5 data. With respect to regional glaciers (GLCR), Zemp et al. (2019) argue that mountain glaciers could vanish entirely by the end of 2100 due to global warming. Moreover, Marzeion et al. (2018) developed a glacier evolution model that quantifies the mass balance change using the partitioning of Farinotti et al. (2019), who examine the majority of the global glaciers and approximate its mass balance and corresponding mean sea level effect. The total impact could be 32 centimeters. Altogether, these detailed examinations motivated us to design the MSL module, which combines the mentioned literature regarding ocean levels.

# Chapter 3

# Theoretical framework

This chapter provides the theoretical background for the methodology of the study. It begins by defining the mathematical mechanism of a tipping point (TP) and introduces the economic damage function that quantifies the chronic physical impact of global warming on GDP growth. Third, Section 3.3 describes the economic output variables analyzed in this study.

## 3.1 Mathematical mechanism of a tipping point

The following paragraphs explain the mathematical process of a TP. First, the qualitative perspective and quantitative view of TPs are described. Third, Section 3.1.3 presents an implication of the mathematics behind TPs.

### 3.1.1 Qualitative Analysis

CTPs are dynamic systems that undergo transitions between stable states by crossing critical threshold values, resulting in sudden regime shifts, bifurcations, or critical transitions (Scheffer et al., 2009). Various natural systems exhibit this behavior, such as epileptic attacks (McSharry, Smith, & Tarassenko, 2003) and financial market crashes (May, Levin, & Sugihara, 2008). Bifurcation theory, introduced by Kuznetsov (2004), describes these phenomena, wherein a small adjustment of a crucial system parameter leads to state changes. Such events occur when the underlying system is in an unstable position characterized by low recovery, meaning it is highly sensitive to external disturbances and may not revert to its previous stable state. In this context, even a minor external perturbation can induce significant changes in the system's dynamics. This concept is illustrated in Figures 3.1a and 3.1b. The left graph shows a minor disturbance that moves the system slightly up the hill but it will return to its stable equilibrium, while the system in the right graph rolls down the hill and transitions to a new state. The basin of attraction represents the unstable region between two equilibria.

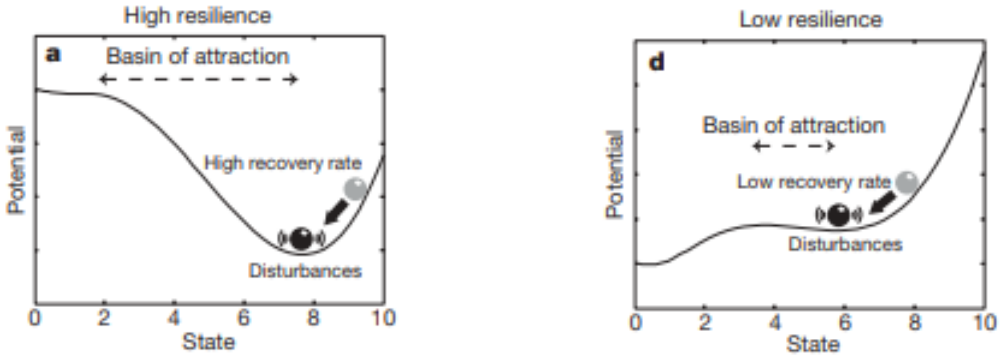


(a) High recovery rate

(b) Low recovery rate

Figure 3.1: Recovery rates of a system, represented by the black dot, that is (a) far from a bifurcation and (b) close to a regime shift. The gray ball is the perturbation. *Adapted from Scheffer et al. (2009).*

### 3.1.2 Quantitative analysis

This section presents a mathematical perspective on bifurcation points. As a system approaches a bifurcation, it enters a lower-dimensional space, known as the normal form, where the behavior of the process is defined (Bury et al., 2021). When the lower-dimensional behavior of the mechanism aligns with the normal form of the bifurcation, a regime shift occurs (Kuehn, 2013). In this case, the system and bifurcation have a codimension of 1, implying topological equivalence. A topological space is a mathematical space where distance between objects exists, for example, the Euclidean.

Another mathematical approach to understanding regime shifts is through the examination of the Jacobian matrix. When the eigenvalues of the Jacobian matrix approach zero, it signifies instability and infinitely slow recovery. This indicates the probable occurrence of a bifurcation.

The most commonly observed bifurcation points are the 'Fold', 'Hopf', and 'Transcritical'. Each of these bifurcations has its own normal form equation and requirements for the Jacobian matrix (Kuznetsov, 2004). The fold bifurcation occurs when the eigenvalues are equal to 0, while the Hopf bifurcation involves a conjugate pair of eigenvalues passing through the imaginary axis. Figure 3.2 depicts the regime jumps associated with these bifurcations. In the case of a Hopf bifurcation, the stable equilibrium transitions to a cycling pattern, while the transcritical bifurcation involves the collision of one unstable state and one stable fixed point, resulting in a shift of stability.

To illustrate a regime shift mathematically, the normal form of a Fold bifurcation is presented by $\frac{dx}{dt} = r - x^2$. Here $r$ represents the critical bifurcation parameter and the system changes states at $r = 0$. The equilibria are found by setting $\frac{dx}{dt}$ to 0, yielding $x = \sqrt{r} \vee x = -\sqrt{r}$. Three scenarios can be considered: for $r > 0$, there are two stable equilibria; for $r = 0$, there is one saddle point, which is the unstable bifurcation point; and for $r < 0$, there are no equilibrium points, leading the system to the basin of attraction. If a dynamic system approaches $r - x^2$ and becomes topologically equivalent,

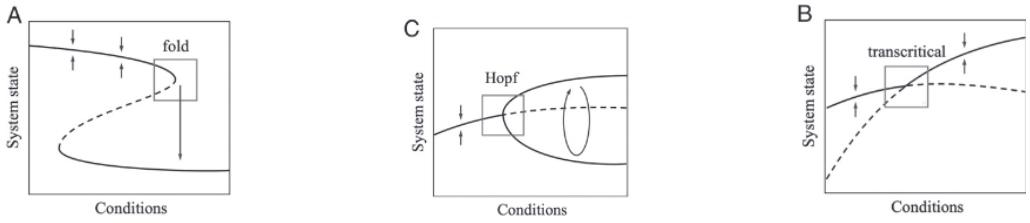


(a) Fold bifurcation (b) Hopf bifurcation (c) Transcritical bifurcation

Figure 3.2: Illustration of bifurcation points. The solid black lines corresponds to stable equilibria and the dashed lines indicate the basin of attraction. *Adapted from Bury et al. (2021).*

it indicates a critical situation and an expected bifurcation.

Most CTPs exhibit fold bifurcations. Conceptually, the x-axis in Figure 3.2a can represent global temperature, and the y-axis can represent a relevant variable, such as the amount of ice on the Greenland ice sheet. However, some CTPs may not follow the complete process depicted in the fold graph, as certain climatic systems may lack the ability to reverse a catastrophic event. Crossing the basin of attraction makes the old equilibrium unattainable.

### 3.1.3 Predicting TP

An emerging area of research focuses on the prediction of critical transitions in natural systems. For instance, the paper of Lade, Tavoni, Levin, and Schluter (2013) investigates processes such as epileptic seizures, while the research of Lenton, Livina, Dakos, Van Nes, and Scheffer (2012) analyzes historical global critical transitions and attempts to predict them. Furthermore, Bury et al. (2021) utilized a modern approach with deep neural networks for forecasting regime shifts.

Another intriguing idea involves autocorrelation modeling. In this case, a parameter that represents the entire dynamic system is identified, and the mechanism can be visualized through the graphs presented in the preceding paragraphs. When the mechanism slows down, the first-lag autocorrelation of this critical parameter increases, causing the graphs to become flat. An autocorrelation value of 1 indicates that the system is no longer changing, and its recovery capability is diminished. Consequently, a sudden external perturbation would force the mechanism to transition between stable states. In recent years, observable critical parameters have been discovered in natural systems, such as the rise in freshwater in the thermohaline circulation (Lenton et al., 2012). As hypothesized, the autocorrelation of this statistic approaches 1, and the parameter's variance increases as the system attains a regime shift.

In conclusion, researchers have proposed various methods for forecasting tipping points. While the findings are promising, these approaches require long-term data and yield projections spanning thousands of years, limiting their applicability to this paper. Nonetheless, this area of climate research

is encouraging and deserves further exploration.

## 3.2 Damage functions

The first study establishing a direct link between climate change and GDP growth is conducted by Nordhaus (1991). Other pioneering works in this field include papers by Ayres and Walter (1991) and Cline (1992). These studies employ diverse mathematical derivations but produce similar outcomes. They estimate the impact of temperature on expected global economic growth. As discussed in Section 2, most climate-related research papers incorporate a regression model that relates GDP growth to temperature and other climate variables. This type of modeling offers interpretability but faces criticism. Keen et al. (2021) argue that these models are inadequate due to methodological flaws. Specifically, they state that climate damage models inaccurately predict the consequences of global warming because they fail to account for several externalities. One example they highlight is the decrease in habitable land, which leads to a reduction in human population and subsequently lowers greenhouse gas emissions. Furthermore, positive developments such as the introduction of innovative techniques are not taken into consideration. Additionally, Rising, Tedesco, Piontek, and Stainforth (2022) point out the neglect of immeasurable risks. As a response, they propose a combination of quantitative and qualitative assessments to incorporate risks that cannot be quantified. Third, the paper of Kemp, Xu, Depledge, and Lenton (2022) emphasizes the focus on worst-case scenarios, arguing that climate damage function papers often overlook lower quantile scenarios that represent extreme outcomes, while these should be examined with caution.

To limit the complexity, this paper does not include external climate impacts. However, it does address the results in the lower path probabilities to amplify the extreme outcomes. The results are generated using an extension of the damage function proposed by Burke and Tanutama (2019), represented by Equation 3.1. Here, $r$ denotes the district, $s$ represents the region type, $t$ symbolizes the time, and $d$ represents the data source for GDP. Moreover, $T$ denotes the temperature, and $P$ represents precipitation. Both variables are introduced as a linear and squared effect, opening the possibility of different impacts for extreme observations. The parameter $\rho_d$ accounts for database-specific effects due to changes in GDP growth, and $\alpha_r$ and $\theta_{st}$ represent the fixed district and time effects, respectively.

$$y_{rsd}(t) = \beta_1 T_{rs}(t) + \beta_2 T_{rs}(t)^2 + \lambda_1 P_{rs}(t) + \lambda_2 P_{rs}(t)^2 + \rho_d + \alpha_r + \theta_s(t) + \epsilon_{rsd}(t) \tag{3.1}$$

## 3.3 Economic variables

To enhance the quality of the research, supplementary economic indicators are incorporated into the final regression analysis. Four specific economic variables: equity returns, inflation rates, long-term interest rates, and unemployment rates, are selected based on previous research to assess the impact of GDP growth rate after accounting for the CTPs. These variables provide insights into financial market responses, price dynamics, borrowing costs, and labor market dynamics resulting from climate impacts. The analysis of these indicators contributes to policy decisions, risk management strategies, and the development of resilient economic systems in the face of climate change.

First of all, analyzing equity returns allows for the evaluation of financial market responses to changes in economic conditions. Extreme weather events and shifts in industry dynamics can influence investor sentiment and market expectations. Shrestha and Subedi (2014) and Singh, Mehta, and Varsha (2011) focused on the equity markets in Nepal and Taiwan, respectively. Their findings show a positive relationship between GDP growth rate and stock market returns. However, most existing literature demonstrates a negative effect. For instance, the study of Fama and French (1989) shows the negative impact of GDP on American equity returns. Furthermore Ritter (2005) obtained a negative correlation of -0.37 between GDP growth and equity returns over the period 1900-2002, arguing that countries with high growth potential do not necessarily offer good equity investment opportunities unless valuations are low. The findings of Dimson, Marsh, and Staunton (2005) confirm this observation through a statistical analysis across 16 countries. With respect to global warming, Bansal, Kiku, and Ochoa (2016), Mescereau (2020), and Bansal, Kiku, and Ochoa (2019) emphasize the importance of investigating the impact of climate change on equity returns through GDP. The results indicate strong negative returns during periods of high temperatures and ocean levels.

Second, inflation is a crucial macroeconomic variable that measures the general increase in prices over time. Understanding the inflationary pressures associated with climate impacts provides insights into cost implications for consumers, businesses, and monetary policy. Climate-related disruptions in agricultural production or resource scarcity can lead to changes in input costs, which in turn affect the prices of goods and services. For example, Friedman (1968) presented an analysis of the role of monetary policy and argues that higher economic growth increases inflation. Additionally, Lim and Sek (2015) applied a vector error correction model. The results show that GDP growth is a significant driving force behind inflation. In periods of high GDP growth, aggregate demand exceeds the supply of goods, and input costs rise due to resource scarcity, resulting in higher inflation rates. Third, Fuhrer and Olivei (2004) used General Method of Moments estimation methods to find a positive relationship as well, but underwrites the importance of other economic variables affecting the inflation rate. In

correspondence with the long-term positive correlation, Odongo, Misati, Kamau, and Kisingu (2022) outline that extreme weather events produce short-term price spikes in African regions.

Next, long-term interest rates play a significant role in determining borrowing costs for businesses and consumers. Analyzing long-term interest rates helps capture the consequences of climate damage on the cost of capital, investment decisions, and economic growth prospects. Changes in economic growth prospects, infrastructure investments, or government policies aimed at addressing climate change can affect investor expectations and risk perceptions, leading to changes in long-term interest rates. The findings of Bernanke, Boivin, and Eliasz (2005) and Dotsey (2012) indicate a positive relation between GDP growth and 10-year interest rates. Central banks respond to higher inflation expectations in booming economies by increasing their short-term interest rates. Also, due to higher expectations on investment returns, investors demand higher interest on loans. These mechanisms are explored further by Weitzman (2007).

Last, the unemployment rate reflects the proportion of the labor force that is unemployed and actively seeking employment. Industries affected by climate-related events may experience job losses or changes in labor demand. On the other hand, climate change can also create jobs by encouraging innovative scientists to develop new techniques to limit global warming. Understanding the impact of climate damage on the unemployment rate provides insights into the short-term labor market dynamics resulting from changes in economic activity. It helps assess the social and economic consequences of climate damage, including the resilience of labor markets and the need for targeted policies to mitigate unemployment risks. According to Okun's law, a 1% increase in unemployment corresponds with a 2% drop in GDP growth. This is emphasized by Levine (2012), who prove that there is a negative correlation between a country's unemployment rate and its economic growth. Periods of growing economies leads to an increase in investment opportunities, encouraging businesses to expand their operations by hiring new employees. In addition, extra consumer spending due to more income and confidence to purchase goods increases the demand for products, which results in more hiring, lowering the unemployment rate. On the other hand, Shimer (2012) argues that the macroeconomic conditions are not the essential factor of unemployment. This opinion is shared by Farsio and Quade (2003). They found that there exists a significant negative correlation between the GDP growth and unemployment rate, but the unemployment rate Granger causes the GDP growth rate and not the other way around. From a climate perspective, the research of Babiker and Eckaus (2007) examines the influence of greenhouse gas emission restriction policies due to global warming and shows that the unemployment rate would increase as a result. Furthermore, Mueller, Gray, and Hopping (2020) states that temperature rising increases migration, thereby elevating the unemployment rate of both the domestic and foreign country. Originally employed immigrated workers do not always find a job.

# Chapter 4

# Data

This chapter outlines the choice of the investigated CTPs and a description of the climate and economic datasets. Finally, the model settings are established with existing literature in Section 4.3.

## 4.1 Selection of Climatic Tipping Points

The list of CTPs is constantly expanding due to new discoveries and the worsening state of the planet. For this research, we adopt the definition of CTPs provided by McKay et al. (2022), which aligns with the IPCC AR6 paper (IPCC, 2022). A CTP is characterized by being self-perpetuating if it surpasses a specific threshold. Once the threshold is crossed, positive feedback mechanisms drive the system towards a different state, and it becomes impossible to return to the previous state. Furthermore, a CTP does not necessarily need to be irreversible, as the dynamic system can eventually return to its initial state. Additionally, the spatial impact of a climate dynamic system must be at least subcontinental, covering an area of approximately 1000 km. On top of this, a CTP must also meet one of the following criteria: 1) it affects global Earth system mechanisms, 2) it impacts the well-being of over 100 million people, and 3) it represents a distinct and critical component of the Earth system.

This paper departs from the study of McKay et al. (2022) by only including CTPs that increase the global temperature. The aim of this research is to demonstrate the negative impact of CTPs on a global scale using a simple and interpretable approach. Therefore, only two climate variables, temperature and mean sea level, are incorporated, following the approach of previous studies (Ayres & Walter, 1991; Burke & Tanutama, 2019; Cline, 1992). Assuming an inverse relation between GDP growth and temperature as well as mean sea level, the inclusion of a destructive CTP that reduces temperature may result in a direct positive impact on GDP growth. This is counter-intuitive because it may cause several other catastrophic disasters such as typhoons, droughts, and catastrophic floods, which are not accounted for in this study. Therefore, the use of these CTPs is not desirable. Similarly, CTPs that

do not impact temperature or mean sea level are excluded from the research as they do not affect the model's outcome. By considering only CTPs that increase global temperature, we have identified 10 CTPs, which are listed in Table 9.2 in the Appendix. Moreover, to provide a geographical overview of these events, Figure 9.1 has been added as well. In the event of new developments or findings, the results in this paper can be easily updated to incorporate additional CTPs as they emerge.

## 4.2 Datasets

The model requires historical climate data for temperature and mean sea level. The entire dataset spans a time period from 1980 to 2022. It is widely accepted in the scientific community that the impact of global climate change has been most vital since 1980 (Foster & Shine, 2002) (J. Hansen et al., 1981) (Pielke, 1998). To enable future predictions, the model also needs projected carbon emissions. Additionally, to compute the impact of CTPs on GDP growth and the other economic indicators, economic data is obtained for 54 different countries. The model has been estimated using panel time series data that accounts for country-specific entities.

### 4.2.1 Climate

To retrieve the historical climate data, two distinct sources are employed. First of all, the atmospheric regional temperatures are extracted from the the CRU dataset of the Climate Change Knowledge Portal (CCKP) (Harris, Osborn, Jones, & Lister, 2020). Second, global mean sea level is obtained from the Climate Science Intelligence Research Organization (CSIRO) dataset, introduced by Church and White (2013) with satellite altimetry. The set consists of high-resolution gridded meteorological and satellite measurements.

Table 4.1: Descriptive statistics of the historical data for the climate variables

| Variable | Obs. | Median | Std. Dev. | Min. | Max. | Skew. | Kurt. |
|---|---|---|---|---|---|---|---|
| Temperature | 43 | 0.89 | 0.25 | 0.48 | 1.38 | 0.24 | -0.91 |
| Mean sea level | 43 | 0.55 | 3.65 | -3.70 | 7.16 | 0.32 | -1.40 |

Temperature is in Celsius, compared to global IPCC 1850-1900 mean. Mean sea level is in centimeters, relative to value in year 2000.

Given the uncertainty surrounding the rate of temperature increase, three greenhouse emission paths are evaluated. For this purpose, the well-established RCP climate sets, introduced by Meinshausen et al. (2011) and utilized by the IPCC in 2016 (IPCC, 2014), are incorporated. The three datasets differ in their projected greenhouse gas emissions, representing various tracks of expected global warming and global abatement. For this research, the RCP2.6, RCP4.5, and the most severe

RCP8.5 dataset are used. The method of simulating temperature and mean sea level from the forecasted greenhouse gas emissions is outlined in Section 5.1.

Descriptive statistics for the historical climate data, consisting of 43 annual observations from 1980 to 2022, are presented in Table 4.1. The distributions of temperature and sea level are similar but at different scales. Notably, there are significant differences between the median temperature and the minimum and maximum temperatures, indicating the presence of outliers. Figure 4.1 illustrates the steady increase in global temperature and mean sea level over time, with an acceleration in recent years. Consequently, the most recent observations in the dataset represent extreme positive outliers, resulting in positive skewness and negative kurtosis. Therefore, Table 4.1 reflects the climate impact of younger generations.

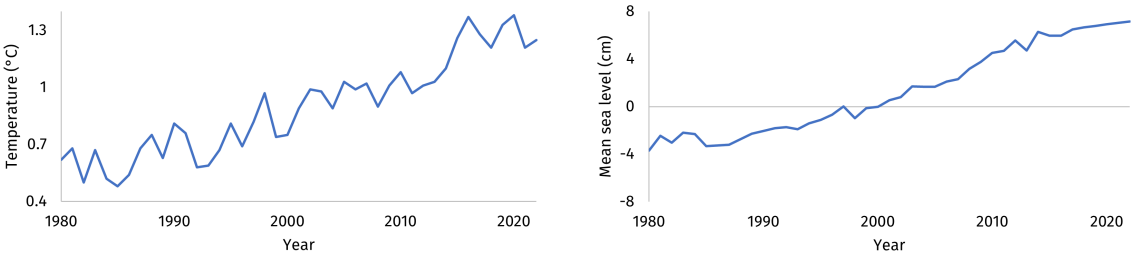


(a) Temperature

(b) Mean sea level

Figure 4.1: The development of the global temperature and mean sea level from 1980 to 2022.

### 4.2.2 Economic

Economic data for each country is obtained from six different organizations in the following order: 1) the International Monetary Fund (IMF), 2) the Organization for Economic Co-operation and Development (OECD), 3) the World Bank Group, 4) Ortec Finance, and 5) the research platforms Macrotrends and 6) Trading Economics. The IMF provides data on GDP growth rate, unemployment rate, and inflation rate (IMF, 2022). The OECD datasets OECD (2023a), OECD (2023b), OECD (2023c), OECD (2023d) and Ortec Finance Ortec-Finance (2023) data are used to extract all four variables. Additional inflation and unemployment data are retrieved from the World Bank World-Bank (2023). Finally, Macrotrends contributes data on GDP (Macrotrends, 2022a) and labor force (Macrotrends, 2022b), while Trading Economics provides information on long-term interest rates (Trading-Economics, 2023).

The data from these sources are combined by selecting the GDP growth rate, inflation rate, and unemployment rate from the IMF, and equity returns and long-term interest rates from the OECD database. Gaps in the data from 1980 to 2022 are filled using data from the most reliable sources in the following order: OECD, World Bank, Macrotrends, Trading Economics, and Ortec Finance. If significant discrepancies occur between two datasets, the observations from the more reliable source

are utilized to minimize database bias. Missing data points are interpolated if at least 90% of the remaining future years are available and no more than two consecutive years are absent. Any regions or observations without GDP growth rate or the other four economic indicators in the historical data are removed. Additionally, series that start after 2008 are eliminated. Last, inflation rate data is winsorized at the 0.5% and 99.5% percentiles to address extreme outliers.

A total of 54 countries are included in the analysis, resulting in 1687 annual observations. Descriptive statistics for the historical economic data are presented in Table 9.2 in Section 9.4 of the Appendix. The table includes a subset of time series representing major economic regions and the emerging country Brazil. The regional median GDP growth rates exhibit small differences, with the median of all countries together, as shown by row *All*, slightly higher. Furthermore, emerging economies, such as Brazil, often display more extreme statistics due to political and regional instabilities. This is evident by Brazil's excess standard deviation and kurtosis for inflation and long-term interest rates. Moreover, Japan stands out with significant variation in inflation, long-term interest rates, and unemployment rates compared to other developed regions, reflecting its unique monetary policy and history of stagflation. Next, the standard deviation of equity series is significantly higher than that of other economic variables, symbolizing its high-risk nature. The table also highlights the minimum and maximum scores for equity components, illustrating extreme losses and gains. The United States, for example, experienced the most extreme loss in the equity index over the past 43 years at -24.2%, compared to a maximum return of 34.4%. Finally, the number of observations varies by region. Some less developed countries have data available from a later starting point, compared to the the developed countries series, which start from 1980 to 2022.

## 4.3 Model settings

The critical temperature values $TA^*$ that trigger the tipping of CTPs are obtained from the study conducted by McKay et al. (2022). Their research involves a comprehensive literature review of various CTPs. It provides estimated temperature values at which these tipping points are likely to occur. Table 4.2 presents the $TA^*$ values derived from their study, along with the minimum and maximum tipping temperatures and the expected temperature impact $I_{TA}$. The uncertainty of temperature estimations on a scale from 0-2, represented by $\upsilon$, is also provided by McKay et al. (2022). Furthermore, the total impact of CTPs on MSL is included in the table based on multiple scientific publications, formulated as $I_{MSL}$. Last, the duration of damage caused by CTPs is denoted as $I_T$.

While creating a CTP correlation matrix is unfeasible due to numerous underlying factors, Rocha et al. (2018) proposed a method to identify interactions using graphical linked structures with three types of connections: *shared driver*, *domino effects*, and *hidden feedbacks*. A *shared driver* connec-

tion indicates that two regime shifts are sensitive to a common global process. A *domino effect* occurs when the likelihood of one CTP changing states increases the probability of another. Third, *hidden feedbacks* represent two-way interactions where both CTPs mutually influence each other.

Table 4.2: The critical estimates for the climate tipping points

| **CTP** | **Min.** $TA^*$ | $TA^*$ | **Max.** $TA^*$ | $\upsilon$ | $I_{TA}$ | $I_{MSL}$ | $I_T$ | **Literature** |
|---|---|---|---|---|---|---|---|---|
| AMAZ | 2.0 | 3.5 | 6.0 | 1 | 0.15 | | 50 | |
| AWSI | 4.5 | 6.3 | 8.7 | 0 | 0.60 | 12 | 10 | Farinotti et al. (2019) |
| EAIS | 5.0 | 7.5 | 10.0 | 0 | 0.60 | 5330 | 10000 | Fretwell et al. (2013) |
| EASB | 2.0 | 3.0 | 6.0 | 1 | 0.05 | | 2000 | |
| GIS | 0.8 | 1.5 | 3.0 | 0 | 0.13 | 728 | 1000 | Aschwanden et al. (2019) |
| GLCR | 1.5 | 2.0 | 3.0 | 1 | 0.08 | 200 | 21 | Farinotti et al. (2019) |
| PFAT | 1.0 | 1.5 | 2.3 | 0 | 0.08 | | 300 | |
| PFTB | 3.0 | 4.0 | 6.0 | 2 | 0.35 | | 25 | |
| TUND | 1.5 | 4.0 | 7.2 | 2 | 0.08 | | 50 | |
| WAIS | 1.0 | 1.5 | 3.0 | 0 | 0.05 | 420 | 2000 | Fretwell et al. (2013) |

$I_{TA}$ (Celsius), $I_{MSL}$ (centimeters), $I_T$ (years), and $\upsilon$ denote the maximum impact on temperature, mean sea level, duration of impact of CTPs, and uncertainty with respect to the $TA$ estimation value, respectively.

Rocha et al. (2018) identified these connections and developed a relation matrix, assigning scores to each type of relation for every combination of CTPs. The shared driver connections are excluded in this study, as they do not reflect direct impacts. The values for the *domino effects* and *hidden feedbacks* are presented in Tables 9.3 and 9.4 in Section 9.5 of the Appendix, respectively. The rows in these tables represent the independent CTP, and the values indicate the strength of the connections. So, a 1 in the second row and first column after the CTP AWSI, indicates that AWSI impacts AMAZ via 1 aspect.

In terms of *domino effects*, there are 19 one-directional interactions between two CTPs. AMAZ is influenced by all other CTPs through one or more factors. For instance, GIS affects AMAZ with four one-sided connections. TUND has the most influence on other CTPs.

In the case of *hidden feedbacks*, the number of connections increases significantly, with the matrix being symmetric due to the two-sided relationships. GIS has substantial global influence, affecting other CTPs, which, in turn, influence GIS again. For example, the two-way interactions between GIS and WAIS amount to 24, as both CTPs are ice sheets and share similar global variables and outcomes. Similar patterns are observed for AWSI and EAIS, with a hidden feedback score of 7.

# Chapter 5

# Methodology

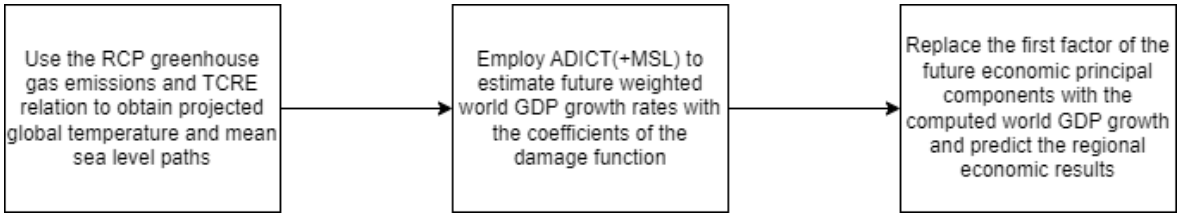


Figure 5.1: A visualization of the methodology applied in this study.

This chapter describes the methodology employed in this study. Figure 5.1 visualizes the mechanism used. The methodology consists of several steps. Step-by-step detailed algorithms are provided in Algorithms 1-3 in Section 9.6 of the Appendix. First, the future temperature paths are projected. According to modern research conducted by Spafford and MacDougall (2020) and IPCC (2022), the relationship between carbon dioxide and temperature is defined by the Transient Climate Response to cumulative carbon Emissions (TCRE). This relationship allows for simulating future temperature paths using only the cumulative $CO2$-emissions. These are available through the predicted RCP datasets (Meinshausen et al., 2011). Each set applies a different emission trajectory.

The second step involves estimating the damage function parameters on the historical climate data. The damage function in this paper is adapted from Burke and Tanutama (2019).

Next, the ADICT module forecasts the impact of CTPs with the projected temperature series. It produces the resulting regional and global GDP growth rates, which are computed with the coefficients of the climate damage function. The ADICT system combines intuitive econometric formulas to form a cohesive structure.

In the fourth phase, the world GDP growth is utilized in the process of simulating the economic indicators per country. To evaluate the effect of CTPs on economic variables via the change in world GDP, the simulation methodology proposed by Steehouwer (2010) is adapted. The choice for this model is based on the relevance and quantity of econometric techniques. Also, the techniques are

interpretable, which makes it appropriate for the audience of this research. The methods consists of a filtering of the economic series into a business cycle and trend domain with the Hodrick-Prescott filter. Afterwards, Principal Component Analysis (PCA) is employed on both the historical domain series. Analysis has shown that the first historical vector of the PCA factors correspond closely with the historical global GDP growth rate (Steehouwer, 2010). Therefore, the first vector is replaced with the historical global GDP growth.

In the future simulation, the PCA factors are projected with their historical Vector AutoRegressive (VAR) characteristics. Additionally, copula theory is applied in combination with Monte Carlo simulation techniques to estimate multiple future scenario paths for the PCA factors. The first vector of the predicted PCA factors is again replaced with the newly projected GDP growth rate, resulting from ADICT, thereby including the damage of the CTPs. In the last step, the economic series are predicted using the future PCA scenario paths and their historical factor loadings.

The following sections explore the generation of the global temperature anomaly and the damage function of this paper. Furthermore, Section 5.3 presents the ADICT module and its MSL extension, which adapts the algorithm for supplementary mean sea level impact. Three models are created: a BASE model that excludes the impact of CTPs, the ADICT system, and the ADICT+MSL model that considers both the temperature and mean sea level effects of individual CTPs. Last, Section 5.4 outlines the methodology utilized to provide the expected regional economic variables.

## 5.1 Data generating process climate data

This paper involves two data generating processes. The first concerns climatic data, which is used as input for the ADICT module, while the second covers the projection of economic data with the influence of CTPs included.

To generate the climate data, required for the ADICT module, the TCRE introduced by Fung, Doney, Lindsay, and John (2005) is employed. This relationship describes the linear connection between cumulative carbon emissions in gigatons (Gt), referred to as the "Carbon budget", and the current temperature increase, called the "warming goal". Matthews, Gillet, and Zickfeld (2009) quantified this relationship and obtained the following equation:

$$TCRE = \frac{Carbon\ budget}{warming\ goal} \tag{5.1}$$

According to Spafford and MacDougall (2020) and IPCC (2022), the TCRE follows a log-normal distribution with a mean of $1.8K$ per $1000Gt\ C$. Using the chemical relation that 3.7 Gt of $CO_2$ equals 1.0 Gt Carbon, the change in temperature can be calculated with Equation 5.2. To generate scenarios for RCP2.6, 4.5, and 8.5, independent observations of TCRE $\sim LN(0.789, 0.24)$ (Spafford

& MacDougall, 2020) are drawn for each of the 1000 scenario paths. These observations are combined with the carbon dioxide emissions from the RCP datasets to compute projected temperatures.

$$TA_A(t) = CO_2(t)/3.7 * TCRE \tag{5.2}$$

Next, the global temperature anomaly compared to the IPCC year 1850-1900 mean, $TA_A(t)$, is utilized for estimating the regional temperatures, defined by Equation 5.3. The global impact of CTPs, denoted as $TA_{CTP}(t)$ is simulated based on activation and impact functions, described in Section 5.3. $TA_r(t)$ represents the definitive regional, $r$, temperature for timestep $t$. It depends on three elements. First of all, the different carbon emission RCP paths produce the global BASE anomaly temperature, $TA_A(t)$, as established by Equation 5.2. Second, the country-specific original starting temperature, $TA_r(0)$ is obtained from the historical data. Third, the aggregate anomaly impact of CTPs, $TA_{CTP}(t)$, is computed with the ADICT+MSL model. Hence, the projected country-specific temperature, $TA_r(t)$, is computed by increasing the starting temperature with the predicted increase in world temperature due to the greenhouse gas trajectories and the temperature rise due to CTPs.

$$\begin{aligned} \Delta TA(t) &= TA_A(t) + TA_{CTP}(t) \\ TA_r(t) &= TA_r(0) + \Delta TA(t) \end{aligned} \tag{5.3}$$

The simulated future temperature values are utilized to estimate the mean sea level using a model proposed by Vermeer and Rahmstorf (2009). This model defines the connection between temperature and mean sea level. The relationship is given by $\frac{dSL}{dt} = a(T(t) - T(0)) + b\frac{dT}{dt}$, with an obtained $R^2$ of 0.99, validating their model. This direct relationship is supported by Figure 5.2, which illustrates the historical relation between the global temperature anomaly and the mean sea level.

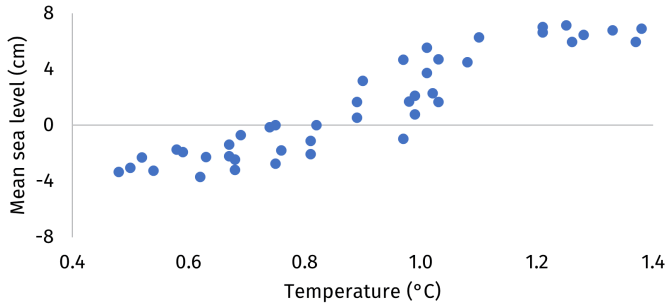


Figure 5.2: A visualization of the linear relationship between temperature and mean sea level.

When the regression of Vermeer and Rahmstorf (2009) is applied on the data in this study, it yields other values. Moreover, there exists regressions that result in an improved $R^2$ and Akaike Information Criterion (AIC), proposed by Hirotugu Akaike in 1973 and examined by Sakamoto, Ishiguro, and Kitagawa (1986). Consequently, built on the ideas of Vermeer and Rahmstorf (2009), the formula in Equation 5.4 reflects the optimal model choice in this paper. $MSL(t)$ symbolizes the

mean sea level anomaly, compared to the year 2000 IPCC benchmark. Furthermore, $\Delta TA(t)$ equals the sum of the global temperature anomaly and the CTP impact, as denoted by Equation 5.3.

$$MSL(t) = -0.76 + 0.94\, MSL(t-1) + 0.76\, \Delta TA(t) + 0.70\, \Delta TA(t-20) + MSL_{CTP}(t) \quad (5.4)$$

The regression produces an $R^2$ of 0.99 and includes a short- and long-term temperature component. As expected, the coefficient for both temperature statistics are positive. Additionally, the coefficient of the first lag of mean sea level is almost equal to 1. Ocean levels do not vary significantly across years. After the projected temperature from the TCRE relation and RCP paths are projected, and after the additional temperature and mean sea level impact of CTPs is incorporated, Equation 5.4 is used to estimate the mean sea level for the 1000 simulation paths.

## 5.2 Damage function

The damage function is shown by Equation 5.5. In the process of including additional (non)-linear transformations of the climate variables in the formula, the AIC statistic and $R^2$ were used as performance metrics. The regression is employed on the historical climate and GDP data of different regions to estimate the parameter coefficients. The step size, $t$, is set to yearly intervals, with $t = 0$ representing the time of model estimation. After including the climate impacts of the CTPs, the damage function is applied to forecast the world GDP growth for 54 countries, denoted as $gdp_r(t)$. Here, $r$ reflects the region.

Regarding the squared temperature term in Equation 5.5, the negative historical regional temperatures, e.g in Canada, remain negative after they are squared by multiplying them with -1 in order to keep the difference with positive squared temperatures.

Also, the first difference is used for $MSL(t)$ in the regression. There are two reasons for this adaption. First of all, the historical ocean level, depicted in Figure 4.1b in Section 4.2.1, shows an almost linear time trend without deviation. Taking the first difference removes this long-term time trend from the data. Second, both the temperature and mean sea level are simultaneously cointegrated, as indicated by a Johansen cointegration statistic (Johansen, 1992) of 20.30 and a corresponding p-value of 0.01. To avoid spurious regressions and non-stationarity, the first difference is taken for the mean sea level. Since the p-value for a cointegration among the first lag of the series is 0.96, the first difference in one of the simultaneous series is sufficient.

Since the analysis involves data with both time and country dimensions, it can be classified as panel data. To avoid omitted-variable bias, a Fixed Effect model is estimated that includes region-specific intercepts. The Fixed Effect estimator is implemented by a time-invariant dummy fixed region effect, which is represented by $\phi_r$.

$$gdp_r(t) = \alpha + \beta_1 TA_r(t) + \beta_2 TA_r(t)^2 + \gamma[MSL(t) - MSL(t-1)] + \phi_r + \epsilon_r(t) \tag{5.5}$$

The parameters are computed through an Ordinary Least Squares regression analysis based on historical data specific to each region. Subsequently, statistical tests are conducted to examine the quality of the residuals of the model. According to the Gauss-Markov theorem, Ordinary Least Squares is the Best Linear Unbiased Estimator with minimum variance under certain assumptions (Harville, 1976). These assumptions are: 1) the error term have zero mean; 2) the residuals are uncorrelated with the independent variables, thus avoiding endogeneity; 3) the errors are uncorrelated with one another, thus avoiding serial correlation; 4) the residuals have a constant variance, thus avoiding heteroskedasticity; 5) there is no correlation coefficient close to one between any two regressors, thus avoiding multicollinearity; and 6) the residuals follow a normal distribution. Each of these restrictions can be tested using existing statistical tests. These tests are explained in Section 9.3 in the Appendix. The damage function is thoroughly tested before it is accepted as one of the dominant formulas in this research. The BASE model only includes the damage function and future predictions of climate and economic variables. The remaining components of the ADICT methodology does not influence BASE.

## 5.3 ADICT

The ADICT structure comprises three key elements. The activation function determines whether a CTP starts to shift regimes. Additionally, the interaction component defines the connections among individual CTPs and influences the activation. Third, the impact formula decides the effect of the activated CTP on temperature.

In each year $t$, the total difference in global anomaly temperature due to the CTPs is estimated. This surplus temperature, compared to BASE, is called $TA_{CTP}(t)$. As stated in Equation 5.3, the total global anomaly temperature is computed by adding $TA_{CTP}(t)$ to BASE $TA_A(t)$. Next, the definitive regional $TA_r(t)$ is predicted by adding this statistic to the original country temperature in 2022. This directly leads to the new global mean sea level through Equation 5.4. Next, the activation functions are utilized to analyze the presence of new bifurcations due to higher global temperatures.

Once the new temperature and ocean level values are estimated with the ADICT module, the regional GDP growth rates are calculated using the damage function described in Section 5.2, denoted as Equation 5.5. The global GDP growth is then computed as the weighted average of the regional economies. Each country's GDP in 2022 is obtained from historical data, and the GDP growth rate weight for each country is calculated as a ratio to the total GDP of all regions combined. For example,

if the GDP in 2022 in the United States is 25 trillion USD and the total summed GDP is 100 trillion, the resulting weight for the United States is 0.25. These regional weights are used in each simulation year to compute a global GDP growth rate based on the country-specific outcomes. The global rate is necessary for the results section and for replacing the first vector of the PCA factors, which determine the economic variable results.

### 5.3.1 Activation

In contrast to the methodology of Rebonato et al. (2022), which uses a logistic function for the climate impact of CTPs, this paper applies a logistic function to estimate the activation of CTPs, given by Equation 5.6. The function approaches an activation value of 0.5 when the future temperature, $\Delta TA(t)$, computed by Equation 5.3, reaches $(TA_i{}^* - z_i(t))$. Unlike current existing literature, a correction for the interactions between CTPs is included. One approach of doing this is to decrease the critical temperature, dependent on the number of the other tipped dynamic climate systems. Consequently, $TA_i{}^*$ is adjusted for the interaction among CTPs by subtracting $z_i(t)$. $z_i(t)$ is calculated with Equation 5.11 and explained in detail in Section 5.3.3.

In addition, a threshold parameter, $\tau \in [0, 1]$, is included in the formula. If the activation statistic, $A_i(t)$ exceeds this value, the regime shift is certain to occur. A low threshold increases the likelihood of regime shifts, leading to a more prudent approach, while a high threshold represents a more conservative approach. Therefore, the parameter choice is a trade-off between prudence and preservation. A sensitivity analysis is conducted to evaluate the impact of different values for $\tau$.

$$\begin{aligned} A_i(t) &= \frac{1}{1 + e^{-\delta_i \left[\Delta TA(t) - (TA_i{}^* - z_i(t))\right]}} \\ 1_i &= A_i(t) \geq \tau \end{aligned} \tag{5.6}$$

Last, the parameter $\delta_i$ determines the activation form of the individual CTP $i$. When a CTP is expected to tip quickly with little uncertainty about the tipping temperature, a steeper shape resembling a binary function around the critical temperature $TA_i{}^*$ is appropriate. This can be achieved by a higher $\delta_i$ value. Equation 5.7 is used to determine the activation scalar. The formula is based on own research and the uncertainty estimates of McKay et al. (2022). Their research not only provides an estimate critical temperature, $TA_i{}^*$, but also minimum and maximum values and an uncertainty statistic of the projections. The coefficients of Equation 5.7 are derived from analysis of the shape of the logistic activation function. The starting point is a steep activation with $\delta_i$ equal to 5 and it decreases as a function of uncertainty and bandwidth between the maximum and minimum tipping point temperature. A wider bandwidth between the maximum and minimum tipping point temperature implies more uncertainty, resulting in a lower $\delta_i$. This leads to a slower activation and the activation starting at an earlier stage. Furthermore, a larger temperature estimation uncertainty, $\upsilon_i$, also reduces

the computed activation scalar, $\delta_i$.

$$\delta_i = 5 - (1 + 0.2 * \upsilon_i) * [(Max.\, TA_i^* - Min.\, TA_i^*)/2] \tag{5.7}$$

### 5.3.2 Damage

The impact of each CTP on the global temperature depends on the values presented in Table 4.2 of Section 4.3. The aggregated temperature change, denoted as $TA_{CTP}(t)$, is computed by summing up the individual CTP effects, $TA_{CTP}(t) = \sum_{i=1}^{N} TA_{CTP,i}(t)$. Because McKay et al. (2022) do not provide definitive information on the tipping process, the impact of each CTP on the temperature is assumed to be linear over time for simplicity.

Equation 5.8 captures the linear relationship and calculates the temperature impact. Here, $I_T$ is the total time span that the CTP affects the temperature, $I_{TA}$ is the maximum impact on temperature, and $t^*$ denotes the time that has passed since the bifurcation of the CTP. The value of $t^*$ is initially 0, and it increments annually after the activation formula has exceeded the threshold parameters, i.e., when $A_i(t) \geq \tau$. We assume that the process of transitioning between states is irreversible until the CTP has completely shifted regimes, as discussed in Section 4.1. Consequently, the impact formula increases temperature till $t^* > I_T$.

$$TA_{CTP,i}(t) = \begin{cases} 0, & A_i(t) < \tau \\ \frac{t^*}{I_T} * I_{TA}, & A_i(t) \geq \tau \cap t^* \leq I_T \\ I_{TA}, & t^* > I_T \end{cases} \tag{5.8}$$

### 5.3.3 Interaction

To measure the interactions between CTPs, the relation scores obtained from Rocha et al. (2018) are converted into a unified interaction statistic using Equation 5.10. The underscore $dom$ represents *domino effects*, while underscore $hid$ denotes *hidden feedbacks*. The domino effects are one-way interactions, allowing the interaction matrix 5.9 to be non-symmetric. However, there are many more two-way relations between CTPs than just a domino effect of one CTP to another. Therefore, $R$ is primarily determined by the hidden feedback relationships between two CTPs. The maximum sum of both scores, represented by $C_{dom} + C_{hid}$, is 100, resulting from the findings of Rocha et al. (2018). The constant $w$ is fixed at 10, chosen such that $\frac{1}{10}\sqrt{100} = 1$.

Equation 5.10 maps the number of relations to an interaction value within the range of $[0, 1]$. The square root function is used to capture the desired shape, with a high derivative for low values that flattens out. Hence, in cases with a low number of connections, the equation still obtains a considerable interaction statistic, and this effect diminishes afterwards. The interaction matrix tends

to approach a symmetric matrix with minor perturbations due to the dominance of hidden feedback connections compared to domino effects.

$$R = \begin{Bmatrix} 1 & \rho_{1,2} & \dots & \rho_{1,N} \\ \rho_{2,1} & 1 & \dots & \rho_{2,N} \\ \vdots & \vdots & \ddots & \vdots \\ \rho_{N,1} & \rho_{N,2} & \dots & 1 \end{Bmatrix} \tag{5.9}$$

$$\rho_{i,j} = \frac{1}{w}\sqrt{r_{i,j}}$$

$$C_{dom} = 80,\ C_{hid} = 20 \tag{5.10}$$

$$r_{i,j} = \frac{\overrightarrow{c_{i,j,dom}} + c_{i,j,hid}}{C_{dom} + C_{hid}}$$

The aggregate interactional measure, $z_i(t)$, is formulated as Equation 5.11. It is a weighted summation of column $i$, which represents CTP $i$, multiplied by the indicator activation functions of the other CTPs. Due to the high degree of uncertainty associated with the effect of one CTP on another, a parameter that reflects the influence of cascading effects is employed. This coefficient, $\omega > 0$, determines the significance of interacting CTPs, where a higher value indicates that the CTPs are more strongly related and, thus, more likely to follow each other. This increases the likelihood that the tipping of one event will result in a chain reaction, which is a matter of serious concern for climate activists. A sensitivity analysis is added to assess its relative impact.

$$z_i(t) = \omega \sum_{\substack{j=1 \\ j \neq i}}^{N} \rho_{j,i} * 1_j \tag{5.11}$$

### 5.3.4 Mean sea level extension

The impact of certain CTPs on the mean sea level can be substantial because they contain massive ice sheets. To account for this, an additional module is incorporated that considers the supplementary volume of water resulting from state changes in five key CTPs: AWSI, EAIS, GIS, GLCR, and WAIS. Given the multitude of factors involved in the estimation of the sea level rise, we drew upon various scientific sources to arrive at the values presented in Table 4.2. As with temperature, the impact of these CTPs on the sea level is determined by their respective activation functions and the impact is modeled similarly as the global temperature change, given by Equation 5.12. This third model, which includes the effect of mean sea level rise, is referred to as ADICT+MSL.

$$MSL_{CTP,i}(t) = \begin{cases} 0, & A_i(t) < \tau \\ \frac{t^*}{I_T} * I_{MSL}, & A_i(t) \geq \tau \ \cap \ t^* \leq I_T \\ I_{MSL}, & t^* > I_T \end{cases} \tag{5.12}$$

## 5.4 Data generating process economic data

Having obtained the projected weighted global GDP growth rate, the economic variables can be projected. First, the Hodrick-Prescott filter, introduced by Hodrick and Prescott (1997), is applied to decompose the historical economic annual data into two frequency domains: a business cycle factor and a trend component. For example, the American equity returns are decomposed into a time serie that reflect the business cycle dynamics and an array that represents the long-term trend effect. Adding both individual series would result in the original historical equity returns. The Hodrick-Prescott filter eliminates a smooth trend from the given data, $y(t)$, by solving Equation 5.13. Here $\xi(t)$ represents the trend and $c(t)$ is the cyclical element. The smoothing parameter $\lambda$ penalizes the acceleration in the trend relative to the business cycle factor. In this study, the optimal parameter value of 6.25 ($\frac{1600}{4^4}$) suggested by Ravn and Uhlig (2002) is used for the annual data.

After the filtering, the business cycle and trend domain series are standardized. To ensure that the future time series approximate to their expected long-term means, the historical means over the period 1980-2022 are added to each of the trend domain observations. For example, the American equity trend domain is standardized with a mean equal to its historical average over 1980-2022.

$$\min_{\xi}(\sum_{t=1}^{T}(y(t)-\xi(t))^2+\lambda\sum_{t=2}^{T-1}[(\xi(t+1)-\xi(t))-(\xi(t)-\xi(t-1))]^2) \tag{5.13}$$

After filtering the economic data into two frequency domains (business cycle and trend), the next step is to apply PCA to reduce the dimensionality of the data. It is assumed that similar economic variables, such as interest rates, across regions are highly correlated and share common features. Moreover, within a country, inflation and unemployment rates, for instance, are closely linked. As a result, the application of PCA on the data yields a small number of generic orthogonal vectors that accurately describe the mechanisms in the data. The PCA factors have dimensions of 43 years, from 1980-2022, times the optimal number of factors for both frequency domains. The optimal number of PCA factors for each domain is determined based on the explained variance, with a minimum threshold of 80%, which is a common threshold value across research (Valle, Li, & Qin, 1999). The first trend PCA vector, which represents the most significant global economic indicator, is replaced with the world GDP growth obtained from the ADICT(+MSL) model to include the impact of CTPs.

Once the historical PCA factors are obtained, the next stage involves simulating these factors into the future. The Yule-Walker method (Yule, 1927) (Walker, 1931), a spectral estimation technique, is used to depict the dynamic behavior of the historical extracted features. The Yule-Walker equations relate the autoregressive model to the autocovariance of the time series. The parameter estimates are approximately equal to a VAR least squares model, but Yule-Walker ensures that the covariance matrix of the model is equivalent to the covariance of the historical data. The formula is given by

Equation 5.14. In the equation, $\gamma_m$ symbolizes the autocovariance function of the data, $\sigma_\epsilon$ represents the standard deviation of the input noise process, $\eta_{m,0}$ is the Kronecker delta function, and $\iota_k$ denotes the autoregressive coefficients. The optimal number of lags to include in this model, $p$, is 1. The use of a VAR(1) model is justified theoretically, as it is shown that a $d$-dimensional stochastic process generated by a VAR(p) can be equivalently represented by an $N \times d$-dimensional process generated by a VAR(1). Therefore, considering a VAR(1) model does not result in a loss of generality.

$$\gamma_m = \sum_{k=1}^{p} \iota_k \gamma_{m-k} + {\sigma_\epsilon}^2 \eta_{m,0} \tag{5.14}$$

When the parameter coefficients are determined, the PCA vectors are simulated through the Monte Carlo method with the use of copula techniques. First, for each of the $f_d$ Yule-Walker equations, the covariance matrix of the residuals is retrieved, denoted as $\Sigma_{F,d}$. This results in a covariance matrix with dimensions corresponding to the number of PCA features in each frequency domains. Next, the Cholesky decomposition method (Benoit, 1924) is utilized to decompose the residual covariance matrices into a lower triangular matrix, $\Sigma_{F,d} = L_d L_d^T$. This ensures that the residuals have a zero mean and a standard deviation of one, which is a standard approach to generate correlated samples through Monte Carlo simulation.

The Gaussian copula is employed to generate future error terms from the Cholesky decomposed triangular matrix, $L_d$. Copulas are commonly used in Monte Carlo simulations to generate correlated random variables. They allow for the construction of joint distributions and the generation of random samples that preserve the desired dependence structure and distribution of real historical data. The Gaussian copula, in particular, can model various types of dependence between variables, from perfect positive correlation to perfect negative correlation. It is suitable for applications in finance, risk management, and other fields where capturing the dependence between variables is crucial. The Gaussian copula function is defined by Equation 5.15, where $\Phi^{-1}$ represents the inverse cumulative distribution of a standard normal, and $\Phi_R$ denotes the joint cumulative distribution of the multivariate normal distribution with correlation matrix $R$. The correlation parameter $\rho$, which determines $R$, is fitted on the residual Cholesky decomposed triangular matrix, $L_d$. This ensures that the sampled error terms have similar characteristics to the original data. Furthermore, the marginal distributions, symbolized as $u_i$, are uniformly distributed on the interval $[0, 1]$. To specify, the copulas are computed separately for both frequency domains, without any linkage between them.

$$C_R^{Gauss}(u) = \Phi_R[\Phi^{-1}(u_1, ..., \Phi^{-1}u_k)] \tag{5.15}$$

After the estimation of the copulas, error terms are sampled for both frequency domains, $bc$ and $trend$, leading to $\chi_{bc}(t)$ and $\chi_{trend}(t)$, respectively. The simulation process continues by applying the PCA simulation equation, shown by Equation 5.16. The formula involves the PCA factor matrix for a

specific domain $d$ at time $t$, denoted as $F_d(t)$. Additionally, $A$ represents the vector with the historical yule-walker VAR coefficients. To provide understanding, the first PCA factor of the business cycle domain is projected each year starting from 2023 with the equation. It multiplies the previous value with the historical VAR coefficient and adds the sampled error term, $\chi_{bc}(t)$, obtained from the copula technique. In the case of the trend domain, the first vector of all future scenario paths of the simulated PCA factors is replaced by the weighted global GDP growth rate resulting from ADICT(+MSL).

$$F_d(t) = \beta + AF_d(t-1) + \chi_d(t) \tag{5.16}$$

In order to enable estimating the future values for the economic variables, the historical economic time series are regressed on the historical PCA features, given by Equation 5.17. Here, $eco_{d,r}(t)$ represents the time series $eco$ of frequency domain $d$ and region $r$. $\phi_{d,r}$ is the economic time series first lag parameter and $B_d$ is the regression coefficient with respect to the PCA factors.

$$eco_{d,r}(t) = \alpha + \phi_{d,r} eco_{d,r}(t-1) + B_{d,r} F_d(t) + \eta_{d,r}(t) \tag{5.17}$$

The same Cholesky decomposition procedure and copula technique is established to generate $\eta_{d,r}(t)$ as for $\chi_d(t)$. The covariance matrix applied has dimensions of 216x216, representing 54 countries times 4 economic variables. With the projected PCA factors and the regression coefficients, the individual region-specific economic data can be computed again for both frequency domains. For each scenario path, the economic variable on frequency domain $d$ is forecasted with the parameter values from Equation 5.17 and the addition of $\eta_{d,r}(t)$. The final economic variable is obtained by adding the two individual domain filtered series: $eco_r(t) = eco_{bc,r}(t) + eco_{trend,r}(t)$. This method is utilized for the equity returns, inflation rates, long-term interest rates, and unemployment rates.

However, due to the error terms, series could exceed the possible value of -100%, and the unemployment rate could become negative, both of which are impossible. To address this, the simulated variables are capped at -100% and the unemployment rate at 0%. Furthermore, to prevent spurious exploding series, a Ridge penalizing policy is implemented on the lag coefficient $\phi_{d,r}$.

To illustrate this process with an example, the historical American equity returns are initially divided in the business cycle and trend domain. Both domains are regressed on the historical obtained PCA factors and the lagged term with Equation 5.17. Next, the parameter outcomes are employed on the future PCA scenario paths, which are generated using their yule-walker VAR relations. This yields 1000 scenarios for the future equity returns. To account for uncertainty and incorporate dependency among the series, error terms are added. These are sampled from the copula methods applied to the residual covariance matrix of the initial economic regression. Finally, the two separated domains are added, resulting in realistic projections of equity returns.

# Chapter 6

# Results

This chapter presents the findings of the conducted research, starting with an examination of the historical parameters of the damage function. A sensitivity analysis is then performed to calibrate the coefficient values with respect to $\tau$ and $\omega$. The global climate impact of three distinct models (BASE, ADICT, and ADICT+MSL) is illustrated in Section 6.3 in relation to different emission paths (RCP2.6, RCP4.5, and RCP8.5). The results are based on 1000 scenarios, spanning a 100-year period from 2023 to 2122. Furthermore, Section 6.4 contains the global and regional GDP growth rates outcomes, along with an analysis of the cumulative long-term effect. Last, predictions for economic variables and the examination of short-term shocks are discussed in Section 6.5.

The final interaction matrix is provided in Section 9.5 of the Appendix. Additionally, Section 9.7 provides an illustrative scenario that helps understanding the influence of CTPs on the global temperature anomaly and global GDP growth.

## 6.1 Damage function

The coefficients for the damage function are tabulated in Table 6.1, estimated based on historical annual data. Four model specifications are employed, selected through evaluation using performance measures such as the AIC statistic and $R^2$. Each model is built on a dataset of 1687 observations.

Among the selected models, the simplest specification denoted as **1** includes only two climate indicators. This model exhibits a low $R^2$ value of 0.02, indicating the presence of omitted variable bias and unexplained variance in the GDP growth rate. In contrast, the **4** model shows an improved performance with an $R^2$ of 0.23 and an AIC value of -7049. The **4** model also outperforms the **2** (-6764) and **3** (-7048) specifications in terms of AIC statistics. Therefore, it is utilized for assessing the impact of CTPs in the subsequent analysis. A comprehensive analysis of the model validity is provided in Section 9.3 in the Appendix. In conclusion, it confirms its adherence to specification

tests, with Newey-West standard errors used to account for serial correlation and heteroskedasticity.

The analysis of the coefficients reveals expected patterns in relation to the temperature statistics. Both the linear temperature parameter and the squared term coefficient display negative values of -2.3 and -0.2, respectively (multiplied by 1000). Additionally, the coefficient for mean sea level is negative (-1.4), indicating a reducing effect on GDP growth rate. These findings confirm that global temperature and mean sea level have a detrimental effect on economic growth. The inclusion of country fixed effects significantly improves the regression model, as indicated by the AIC statistic and $R^2$.

Table 6.1: Linear regression results for the relationship between GDP growth and climate

| **Variable** | **1** | **2** | **3** | **4** |
|---|---|---|---|---|
| $TA$ | 0.5*** | -1.0*** | -5.9*** | -2.3 |
| | (0.1) | (0.3) | (1.2) | (2.2) |
| $TA^2$ | | 0.1*** | | -0.2* |
| | | (0.0) | | (0.1) |
| $MSL(t) - MSL(t-1)$ | -1.1 | -1.1 | -1.1 | -1.4 |
| | (1.2) | (1.2) | (1.0) | (1.0) |
| Countries-effect | Exc. | Exc. | Inc. | Inc. |
| Observations | 1687 | 1687 | 1687 | 1687 |
| $R^2$ | 0.02 | 0.03 | 0.23 | 0.23 |

*Note*. Coefficients and standard errors are multiplied with 1000;

Standard errors are in parentheses; * $p < 0.1$, ** $p < 0.05$, *** $p < 0.01$

## 6.2 Parameter sensitivity analysis

To evaluate the sensitivity of the model to variations in its free parameters, the global GDP growth rate generated by the ADICT+MSL model is examined. Figure 6.1 presents the outcomes for the parameter $\tau$. The individual lines depict the paths of the percentage Value-at-Risk (VaR) of the weighted world GDP growth. It is evident that a more conservative tipping threshold leads to an increase in the expected global GDP growth rates. When $\tau$ is set to 1.0, representing a scenario without any bifurcations, the median global GDP growth rate is 2.4%, compared to -0.8% when all CTPs shift regimes at $t = 0$. These extreme cases are clearly discernible from the steep incline at the beginning and end of the figure. The GDP growth rates for $\tau$ values of 0.05 and 0.95 are 1.0% and 1.5%, respectively.

Figure 6.1b displays the standard deviation of the GDP growth rate, exhibiting an interesting pattern of volatility. This trend is evident in the differences between the 97.5% VaR and 2.5% VaR. Initially, the gap between the two curves increases to shrink afterwards. This suggests that a higher

probability of regime shifts, represented by lower values of $\tau$, leads to approximately equivalent outcomes across all scenarios due to similar CTPs changing states and identical timing of bifurcations. Conversely, increasing $\tau$ further from 0.4 decreases the standard deviation, as it reduces the number of regime shifts and consequently produces fewer temperature shocks.

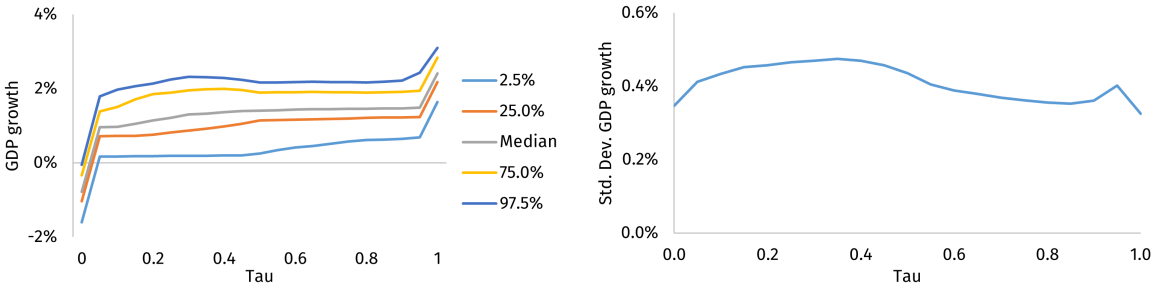


(a) Return (b) Standard deviation

Figure 6.1: The median and standard deviation of the ADICT+MSL projected global GDP growth rate with the RCP4.5 path in 2122 for different values of $\tau$.

Moving on to the interaction coefficient, $\omega$, as illustrated in Figure 6.2, it is observed that it does not significantly influence the model's outcome. The decline in the GDP growth rate resulting from enhanced interaction among different CTPs is merely 0.1 percentage points for the two most extreme values of $\omega$ examined. Although the VaR curves slightly deviate from the median for larger connection coefficients, the overall effect is not substantial.

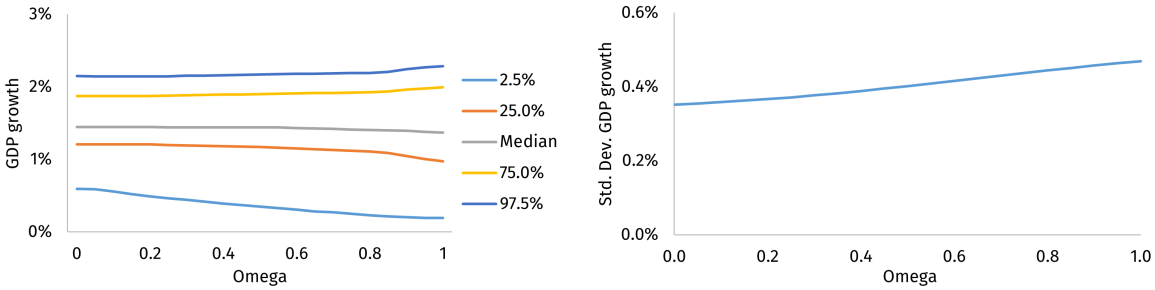


(a) Return (b) Standard deviation

Figure 6.2: The median and standard deviation of the ADICT+MSL projected global GDP growth rate with the RCP4.5 path in 2122 for different values of $\omega$.

In terms of standard deviation, the observations indicate a linear increasing trend. Greater interaction among the CTPs leads to more state changes, resulting in a higher frequency of temperature shocks. However, the increase in volatility for the extreme statistics of $\omega$ is only 0.1 percentage points.

In conclusion, the parameter $\tau$ plays a critical role in determining the outcomes of the ADICT+MSL model. A slightly cautious yet balanced approach is adopted, setting $\tau$ at 0.4. Contrarily, the impact of $\omega$ is not significant. Therefore, $\omega$ is fixed at 1.0 for the purpose of this analysis.

## 6.3 Climate impact

The next paragraphs describe the effect of CTPs on the global anomaly temperature and mean sea level. First, the climate results are explored for each of the RCP paths when employing the BASE model. Second, Section 6.3.2 evaluates the relative outcomes of the ADICT(+MSL) models.

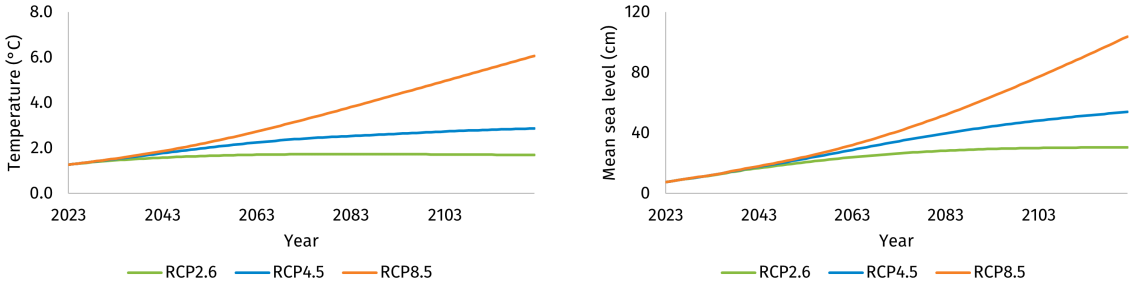


(a) Temperature

(b) Mean sea level

Figure 6.3: The BASE global temperature and mean sea level projections for the RCP datasets.

### 6.3.1 BASE

The temperature is determined using the TCRE relationship specified in Equation 5.2 in Section 5.1. Additionally, mean sea level is computed using Equation 5.4. Figure 6.3 illustrates the median values of temperature and mean sea level for the BASE model, which are independent of ADICT and ADICT+MSL. The figure shows that temperature and mean sea level exhibit a similar trend. This alignment can be attributed to the data generation process of the mean sea level variable, which involves a linear combination of past mean sea level and historical and simultaneous temperature observations.

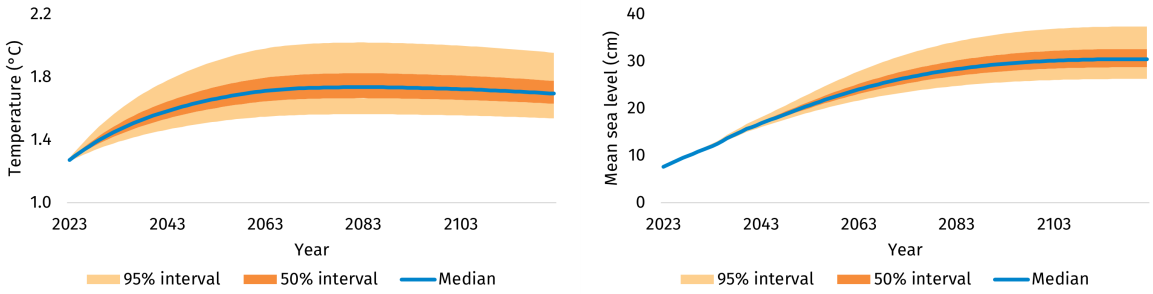


(a) Temperature

(b) Mean sea level

Figure 6.4: BASE anomaly temperature and mean sea level for the RCP2.6 emission path.

Until 2035, the temperature and mean sea level values for the three emission paths (RCP2.6, RCP4.5, and RCP8.5) produce relatively similar trends. However, their trajectories diverge significantly thereafter. In 2035, the median temperature values for the respective scenarios are projected to reach 1.5, 1.6, and 1.6 degrees Celsius, while mean sea level is projected to rise to 13.0, 13.3, and

13.4 centimeters, respectively. By 2080, the temperature values for the three scenarios are projected to increase to 1.7, 2.5, and 3.7 degrees Celsius, accompanied by mean sea level rises of 28.4, 38.8, and 49.0 centimeters. At the end of the simulation period, in 2122, the global temperature is expected to rise to 1.7 degrees Celsius for RCP2.6, 2.9 degrees Celsius for RCP4.5, and 6.1 degrees Celsius for RCP8.5. Correspondingly, mean sea level is projected to increase to 31.4, 55.2, and 104.9 centimeters above the global mean sea level of 2000, respectively. As anticipated, the RCP8.5 scenario, representing the most severe emissions pathway, results in the largest temperature increase and mean sea level rise. The temperature appears to continue increasing beyond the simulated 100-year period.

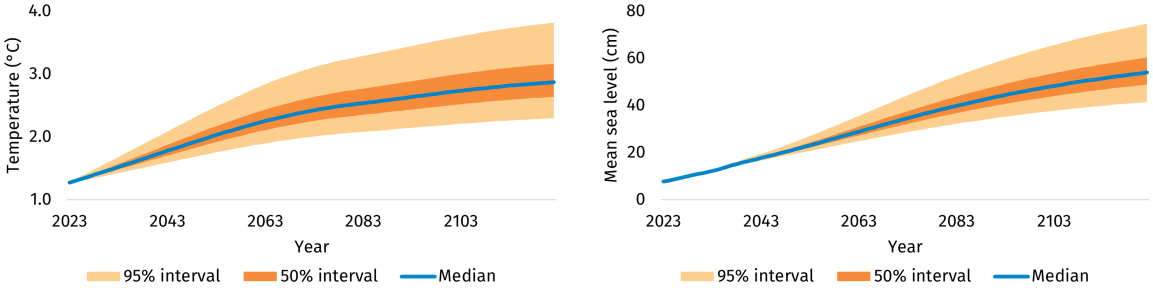


(a) Temperature

(b) Mean sea level

Figure 6.5: BASE anomaly temperature and mean sea level for the RCP4.5 emission path.

For a more detailed examination of the scenarios, Figures 6.4-6.6 provide additional insights into 1000 individual scenarios for each emission path. The deviation in the graphs comes from the log-normal distribution and the cumulative greenhouse emissions. As a result, the scenario clouds widen over time, reflecting the inherent uncertainty associated with future carbon emissions. The dependence on past data contributes to the widening of the bands. For instance, in 2035, the 50% interval width for the RCP4.5 emission path is 0.1 degrees Celsius, while it expands to 0.4 degrees Celsius by 2080. Similar trends can be observed for the 50% interval bandwidths of mean sea level, which increase from 0.4 centimeters in 2035 to 6.6 centimeters in 2080.

Furthermore, the scenario clouds for the RCP2.6 emission path exhibit the least dispersion. In 2080, the 95% interval width is 0.5 degrees Celsius for the RCP2.6 path, compared to 2.4 degrees Celsius for the RCP8.5 climate scenarios. In terms of mean sea level, the difference between the $97.5^{th}$ and $2.5^{th}$ percentiles amounts to 9.6 centimeters and 30.5 centimeters, respectively.

Moreover, it is important to note that for each emission path, there is considerably more undesired upside risk. This pattern arises due to the positive skewness of the log-normal distribution of the TCRE parameter, as discussed in Section 5.1. This is evident from the smaller absolute difference between the 97.5% VaR and the median, compared to the 2.5% VaR and the median. For the RCP2.6, RCP4.5, and RCP8.5 datasets, the 97.5% VaR is located 0.3, 1.2, and 3.5 degrees above the median, whereas the 2.5% VaR lies 0.2, 0.6, and 1.7 degrees Celsius below the median. This behavior

highlights the tail risk associated with global warming.

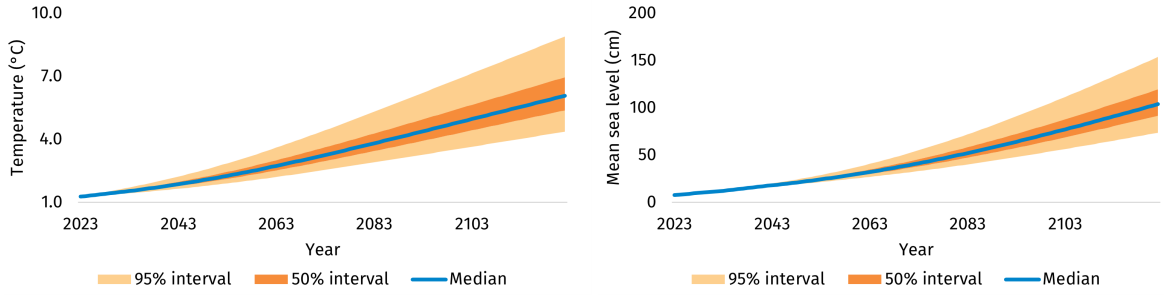


(a) Temperature

(b) Mean sea level

Figure 6.6: BASE anomaly temperature and mean sea level for the RCP8.5 emission path.

### 6.3.2 ADICT(+MSL)

Figures 6.7-6.9 provide visualizations of the changes in temperature anomaly ($\Delta TACTPs$) and mean sea level anomaly ($\Delta MSLCTPs$) resulting from the ADICT and ADICT+MSL modules. Note that the mean sea level is a function of the previous mean sea levels. Therefore, the additional impact of CTPs can be more than tabulated in Table 4.2 in Section 4.3 due to a compounding effect.

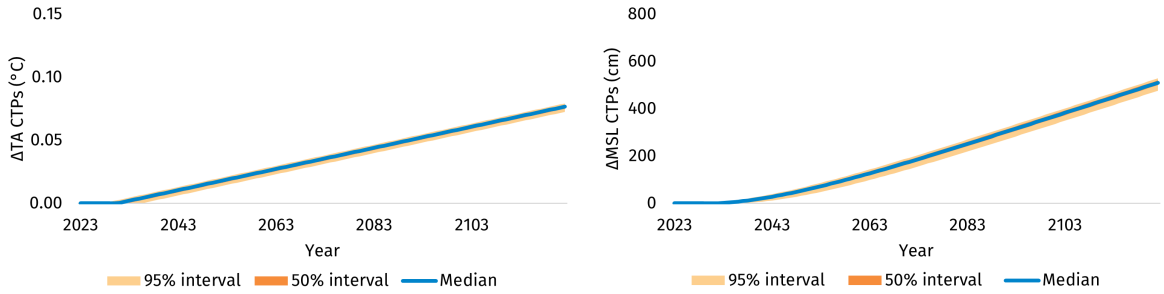


(a) Temperature

(b) Mean sea level

Figure 6.7: ADICT+MSL relative temperature and ocean level increase for the RCP2.6 emission path.

Starting with Figure 6.7, it shows that the additional temperature increase for the RCP2.6 emission path is relatively small, with a negligible increase of less than 0.1 degrees Celsius in 2122. Also, the dispersion around the median is minimal. However, there is a significant rise in mean sea level over time. Following the bifurcations in GIS, GLCR, and WAIS, the ocean level starts to rise, indicating the global implications of these CTPs. The total additional rise in mean sea level above the BASE model after 100 years of simulation amounts to 510.1 centimeters. This substantial increase would lead to extensive flooding, damage to infrastructure, population migration, and loss of ecosystems. The lower and upper bands of the distribution do not show extreme outliers compared to the median, suggesting that these projected ocean levels are likely to occur across a range of scenarios, which is a matter of concern.

Next, focusing on Figure 6.8, there is a considerable greater divergence in temperature starting

from the year 2060. This coincides with the tipping of the AMAZ in certain scenarios, triggering a chain reaction that causes the tipping of PFTB and TUND to tip as well. By the end of the simulation period, the 95% interval is $[0.1, 0.9]$ degrees Celsius around the median of 0.2. Consequently, in the 5% best-case scenarios, the additional temperature increase remains little, while in the worst-case scenarios, it escalates to an extra 0.7 degrees Celsius on a global scale. This observation underscores the potential dangers associated with climate impact in the upper tails. In terms of mean sea level, the graph exhibits a similar pattern as the RCP2.6 emission path because the tipping of EASB, PFAT, and TUND does not involve ice mass melting.

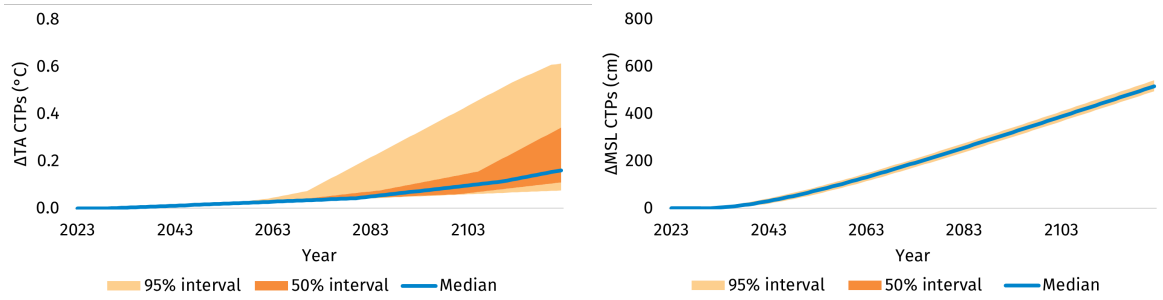


(a) Temperature

(b) Mean sea level

Figure 6.8: ADICT+MSL relative temperature and ocean level for the RCP4.5 emission path.

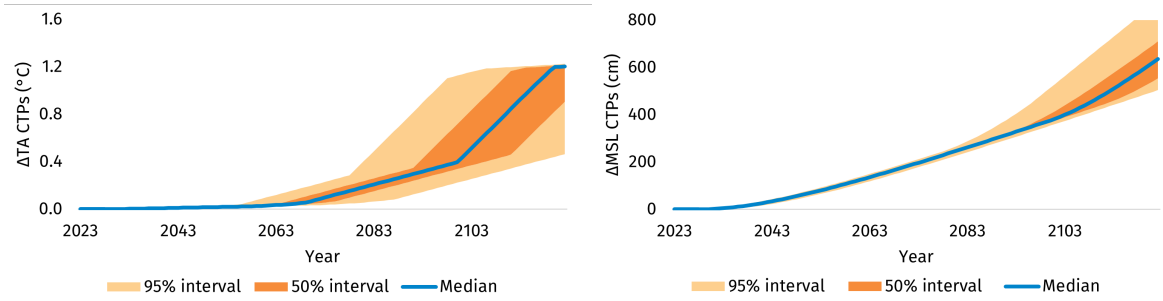


(a) Temperature

(b) Mean sea level

Figure 6.9: ADICT+MSL relative temperature and ocean level for the RCP8.5 emission path.

Last, considering the most severe RCP8.5 dataset, greater disparities emerge among the 1000 scenarios. The same pattern observed in Figure 6.8a is also present in Figure 6.9a, but it occurs at an earlier stage in the simulation process. Furthermore, due to the higher expected temperature, the AWSI undergoes a regime shift as well, leading to a substantial increase in relative temperature and further divergence from the median. In 2122, the 2.5% VaR is 0.5, while the 97.5% VaR corresponds to an additional 1.5 degrees Celsius. The median temperature resulting from ADICT is projected to be 1.2 degrees Celsius above the 6.1 degrees Celsius estimated by the BASE model, representing a 19.8% increase. Moreover, the median mean sea level rise established by ADICT+MSL, is 635.3 centimeters with a corresponding 95% interval in 2122 of $[504.4, 961.4]$ centimeters. Compared

to both the RCP2.6 and RCP4.5 datasets, the bifurcation in AWSI and EAIS for some worse-case scenario paths results in a significant additional impact on ocean levels. To provide context, a 6-meter rise in ocean levels would result in the flooding of approximately one-third of Florida, while a 10-meter rise would have devastating consequences for New York (Brouillette, 2023).

## 6.4 GDP impact

This section provides the GDP outcomes with focus on CTP impact, applying the BASE, ADICT, and ADICT+MSL models. It includes an examination on the long-term cumulative effect on GDP and additional analysis to examine the effect on individual regions.

### 6.4.1 Global

Table 6.2 displays the outcomes for the BASE, ADICT, and ADICT+MSL models across different RCP paths. These model-RCP combinations are visually depicted in Figure 6.10 for BASE in Section 6.4.1.1. The relative supplementary impact for ADICT and ADICT+MSL are provided in Figure 6.11. Third, Section 6.4.1.3 outlines the non-relative effect of ADICT+MSL.

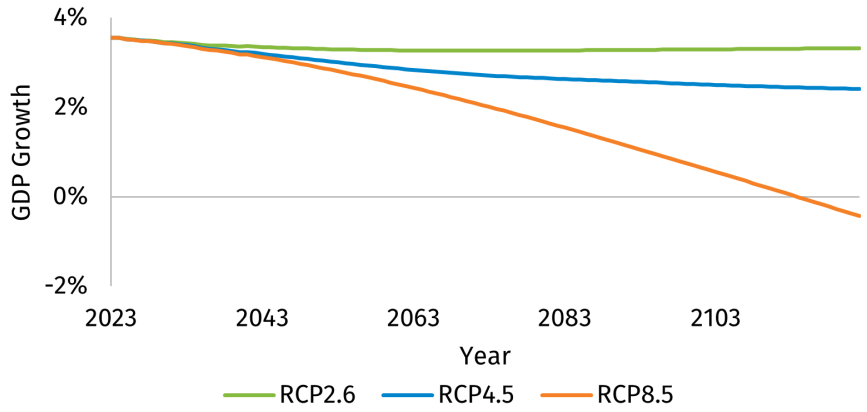


Figure 6.10: Median of the GDP growth rate with BASE for the RCP sets.

#### 6.4.1.1 BASE impact

Regarding Figure 6.10, the BASE results align with the anticipated patterns. The temperature and mean sea level rise in the RCP2.6 emission path remain relatively low, illustrated by Figure 6.3a and 6.3b in Section 6.3, resulting in a stable future GDP growth rate. Additionally, the climate graph exhibits a decline of temperature and ocean levels after 50 years of simulating. This is translated into a slightly higher GDP growth as well. Similarly, matching patterns can be observed for the RCP4.5 and RCP8.5 data. Both lines present the inverse values of the climate variables.

Second, as expected, the RCP8.5 emission trajectory, which involves higher carbon dioxide emissions, exhibits the most significant damage. The GDP growth rate reduces from 3.6% to -0.4%, com-

Table 6.2: Weighted global GDP growth rates with 1000 projected scenarios for BASE, ADICT, and ADICT+MSL, employed on each of the three IPCC emission paths over the period 2023-2122.

| Model | Emission path | Measure | 2023 | 2043 | 2063 | 2083 | 2103 | 2122 |
|---|---|---|---|---|---|---|---|---|
| BASE | RCP2.6 | Median | 3.6% | 3.3% | 3.3% | 3.3% | 3.3% | 3.3% |
| | | Std. Dev. | 0.0% | 0.1% | 0.1% | 0.1% | 0.1% | 0.1% |
| | RCP4.5 | Median | 3.6% | 3.2% | 2.8% | 2.6% | 2.5% | 2.4% |
| | | Std. Dev. | 0.0% | 0.1% | 0.2% | 0.3% | 0.3% | 0.3% |
| | RCP8.5 | Median | 3.6% | 3.1% | 2.4% | 1.5% | 0.6% | -0.4% |
| | | Std. Dev. | 0.0% | 0.1% | 0.3% | 0.6% | 0.9% | 1.2% |
| ADICT | RCP2.6 | Median | 3.6% | 3.3% | 3.2% | 3.2% | 3.2% | 3.3% |
| | | Std. Dev. | 0.0% | 0.1% | 0.1% | 0.1% | 0.1% | 0.1% |
| | RCP4.5 | Median | 3.6% | 3.2% | 2.8% | 2.6% | 2.4% | 2.3% |
| | | Std. Dev. | 0.0% | 0.1% | 0.2% | 0.3% | 0.4% | 0.5% |
| | RCP8.5 | Median | 3.6% | 3.1% | 2.4% | 1.4% | 0.1% | -1.6% |
| | | Std. Dev. | 0.0% | 0.1% | 0.3% | 0.7% | 1.2% | 1.4% |
| ADICT+MSL | RCP2.6 | Median | 3.6% | 2.9% | 2.5% | 2.4% | 2.3% | 2.4% |
| | | Std. Dev. | 0.0% | 0.1% | 0.1% | 0.1% | 0.1% | 0.1% |
| | RCP4.5 | Median | 3.6% | 2.7% | 2.0% | 1.7% | 1.5% | 1.4% |
| | | Std. Dev. | 0.0% | 0.1% | 0.2% | 0.3% | 0.4% | 0.5% |
| | RCP8.5 | Median | 3.6% | 2.6% | 1.6% | 0.5% | -1.1% | -3.4% |
| | | Std. Dev. | 0.0% | 0.2% | 0.3% | 0.7% | 1.6% | 1.8% |

pared to 2.4% for the RCP4.5 data. Hence, if the world continues following the RCP4.5 path, even without the existence of CTPs, the decrease in annual global GDP would amount to 1.2 percentage points, equivalent to a 32.3% drop relative to the initial value in 2022.

Furthermore, the standard deviations provided in Table 6.2 increase over time, indicating growing uncertainty as the simulation progresses into the future. In 2122, the deviations are 0.1%, 0.3%, and 1.2% for the RCP2.6, RCP4.5, and RCP8.5 paths, respectively, in contrast to 0.1%, 0.1%, and 0.1% in 2043. Moreover, notice that higher carbon emissions lead to greater dispersion in the results, as presented by the higher volatilities associated with the RCP8.5 scenario compared to RCP2.6.

Fourth, it is important to observe that the standard deviations for ADICT+MSL are larger compared to those for ADICT and BASE models due to the inclusion of CTPs and resulting GDP shocks. For instance, when employing the RCP8.5 trajectory, the volatility in weighted GDP growth is 1.8% with ADICT+MSL, representing a 0.6 percentage point increase compared to the BASE model.

#### 6.4.1.2 ADICT+MSL relative damage

Figures 6.11a to 6.11c depict the relative values of the weighted GDP growth rates for ADICT and ADICT+MSL compared to the BASE model, highlighting the impact of CTPs. The results indicate that CTPs affecting only global temperature do not exert a significant effect for the RCP2.6 and RCP4.5 scenarios. The difference between BASE and ADICT remains below 0.2% for both trajectories, corresponding with a decrease of 1.8% and 5.6%, respectively. On the other hand, the impact of CTPs in the most severe RCP8.5 set is significant, leading to an additional drop of 1.2 percentage points on top of the -0.4% annual rate, predicted by BASE.

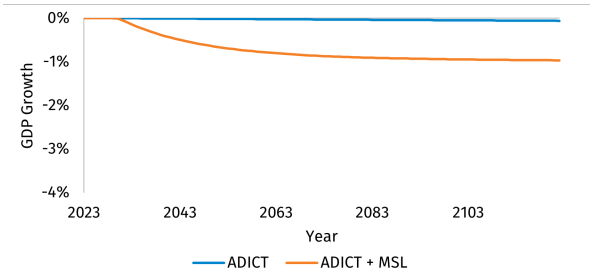


(a) RCP2.6

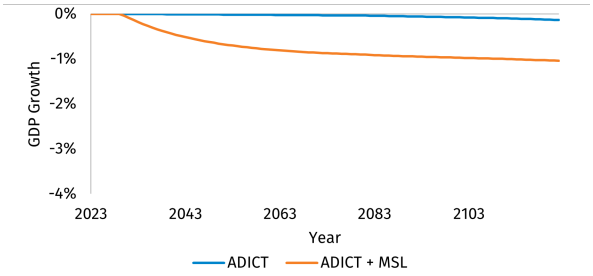


(b) RCP4.5

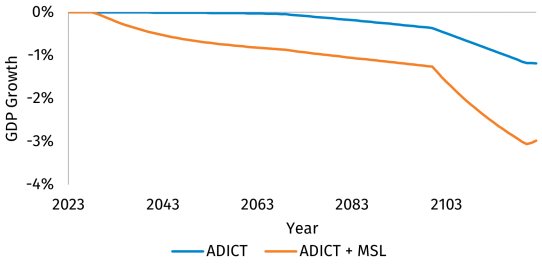


(c) RCP8.5

Figure 6.11: GDP growth rates of ADICT and ADICT+MSL, relative to BASE.

Next, including the impact of the massive ice sheets with ADICT+MSL in the estimation leads to a considerable reduction in global GDP growth. The annual economic growth rate declines for BASE. The difference in growth rate between 2122 and 2023, matches 0.2%, 1.1%, and 4.0% for the three RCP paths. The additional decrease due to the supplementary mean sea level effect of the CTPs is 1.0, 1.0, and 3.0 percentage points, respectively, underscoring the importance of CTPs.

#### 6.4.1.3 ADICT+MSL scenario clouds

Figure 6.12 presents the scenario clouds of ADICT+MSL for the three emission paths, illustrating the absolute predicted annual GDP growth rates instead of the relative values. In the case of the RCP2.6 path, the effect of GIS, GLCR, and WAIS is evident. The initial decline around 2035 is triggered by their bifurcations. Over time, the dispersion remains minimal, implying a limited number of additional bifurcations and negligible impact. Consequently, the 95% confidence interval in 2122 is narrow with the bounds at $[2.2\%, 2.5\%]$.

Regarding Figure 6.12b, a considerable decline can be observed. The median GDP growth rate drops from 3.6% to 1.4%, while the standard deviation increases over time. At the end of the simula-

tion horizon, the 2.5% VaR and 97.5% VaR are 0.2% and 2.3%, respectively. Again, the wider lower bandwidth demonstrates the substantial negative downside risk associated with global warming.

Last, the RCP8.5 graph presents the most extreme outcomes. The 95% confidence interval amounts to $[-6.8\%, -0.1\%]$, centered around the median value of -3.4%. The additional impact of AWSI is illustrated by the sharp decline from 2090. The projected negative annual GDP growth would lead to inhumane conditions worldwide, resulting in chaos, and catastrophes, which could decimate the global population. Therefore, it is crucial that the international community takes preventive measures to avoid such scenarios.

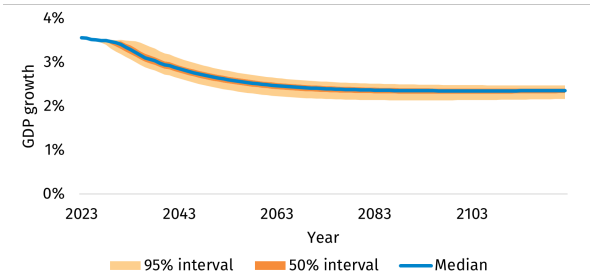


(a) RCP2.6

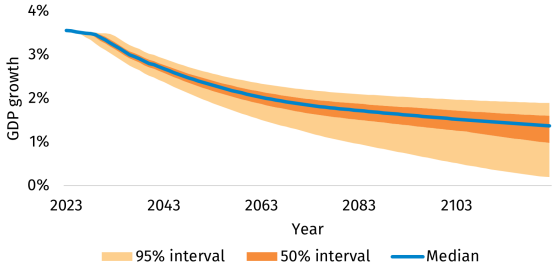


(b) RCP4.5

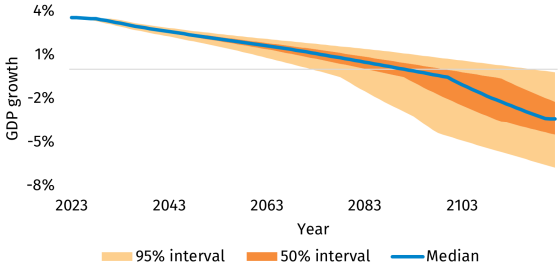


(c) RCP8.5

Figure 6.12: ADICT+MSL GDP growth scenarios.

### 6.4.2 Long-term cumulative impact

Figure 6.13 illustrates the long-term impact of CTPs on the cumulative GDP. While the annual weighted GDP growth rate of the RCP2.6 path stays fixed over time, due to the compounding effect, the cumulative GDP series increase exponentially over time. The cumulative GDP in 2122 equals 1305.7%.

On the other hand, the economic growth declines substantially with the RCP8.5 data. In 2091, the cumulative GDP starts dropping. The final cumulative GDP is 211.9%, which is less than one-fifth of the RCP2.6 emission trajectory, indicating the long-term damage of global warming.

Third, the economic situation of the RCP4.5 does improve over time. The GDP ends at 789.8%. This represents a 515.8 and 577.9 percentage point difference with the RCP2.6 and RCP8.5 path, respectively, indicating the extreme varying world outcomes with respect to the different climate tracks.

### 6.4.3 Regional

Figure 6.14 presents world maps, illustrating the results for three different simulation years with ADICT+MSL applied to the RCP4.5 dataset. Over time, the GDP growth rate gradually decreases, resulting in a red-colored world map. The most significant declines in annual GDP growth rates are experienced for China, India, and Indonesia. Their initial GDP growth of 8.7%, 6.2%, and 5.5% decreases to 0.8%, -0.4%, and -0.5%, respectively. Moreover, the average GDP growth among all 54 regions declines by 2.4 percentage points, from 2.8% till 0.3%, over the simulation horizon. Consequently, in 2122, 16 countries exhibit negative GDP growth rates.

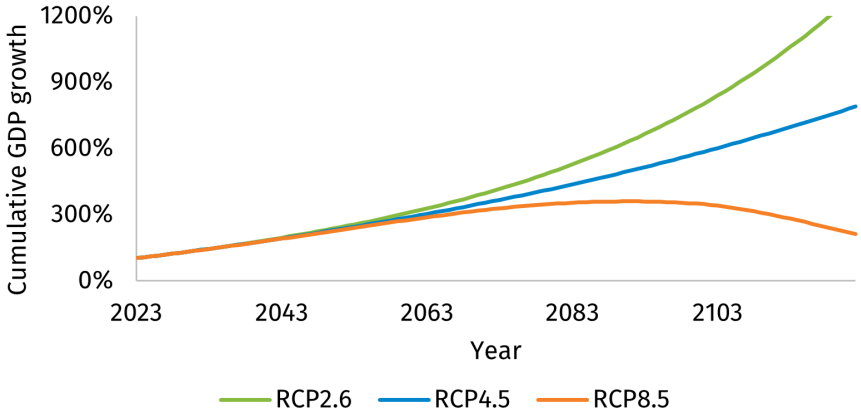


Figure 6.13: Cumulative GDP with ADICT+MSL on the RCP sets


(a) 2023 (b) 2073 (c) 2122

Figure 6.14: World map of GDP growth rate with ADICT+MSL employed on RCP4.5.

Furthermore, the results indicate that the effect of global warming varies across countries based on their local temperature conditions. This is evident in the dark-red colors of the Southern hemisphere, which is considered warmer than the Northern locations. For instance, the lowest GDP growth rates are estimated for the hottest regions Nigeria, Singapore, and Thailand with annual rates of -0.6%, -0.7%, and -0.6%, respectively. Contrarily, the coldest countries, Canada, Iceland, and Russia exhibit projections of 1.7%, 1.2%, and 1.6%. This result reflects the vulnerability of warmer countries. This is intuitive because certain geographical locations would become uninhabitable if the temperatures keep rising due to heat exhaustion, water scarcity, and crop failures.

Moreover, the world maps suggest that developed regions are less impacted by climate change and

CTPs, whereas emerging regions face greater challenges. This outcome may be attributed to the lower temperatures in the more developed regions. Nevertheless, it is a cause for concern, as less developed regions often have limited resources and weaker infrastructure, making it more difficult to cope with the consequences of catastrophic climate events such as floods, crop failures, and earthquakes.

## 6.5 Economic impact

As outlined in Section 5.4, the initial step in simulating the economic variables involves filtering the historical data into business cycle and trend components. Subsequently, the number of principal components are computed, and the future PCA factors are then projected using copula theory, the Monte Carlo method, and the Cholesky decomposition of the error covariance matrix. Finally, the future economic series are generated using the regression coefficients derived from Equation 5.17.

With a threshold criterion of 0.80 for the $R^2$, 9 principal components are selected for the business cycle and 3 principal components for the trend frequency domain. Notice that the first principal component of the trend vectors is replaced with the weighted global GDP growth rate obtained from the ADICT(+MSL) module. Due to the inter-dependency between the time series, established by the methodology of Steehouwer (2010), the economic indicators are influenced not only by the GDP growth rate but also by their mutual relationships.

The impact of the integrated model on the economic outcomes is presented in the following paragraphs. First, the results are examined on global level. Next, the short-term shock of a selection of CTPs is explored. Last the regional changes in economic variables are analyzed.

### 6.5.1 Global

The economic indicators are demonstrated in Figures 6.15-6.17 for the three emission trajectories. The BASE and ADICT models exhibit similar outcomes, while ADICT+MSL displays distinct results due to significant differences in world GDP growth rates derived from the MSL module. Therefore, in the remaining text, only BASE and ADICT+MSL are explored.

Starting with the RCP2.6 dataset in combination with BASE, the anticipated economic patterns during periods of relative climate stability and calm financial times are depicted. Global equity returns are estimated to rebound from the current negative outlooks to positive values. Additionally, the extreme inflation rates are projected to recover and converge towards 3.5%. As a reaction to the current elevated inflation rates, the model predicts a temporary increase in the long-term interest rates, followed by a stabilization at 4.3%. Moreover, the Okun's law suggests that GDP growth and unemployment are inversely related. Consequently, the unemployment rate increases slightly due to lower expected economic growths. However, the increase is only 0.5 percentage points.

On the other hand, when examining the ADICT+MSL results, which incorporate the lower GDP growth rates enforced by CTPs, distinct trends are observed. With respect to equity returns, they exhibit a decline after the initial rebound, which indicates that a lower GDP growth rate corresponds with lower equity returns. The projected equity return in 2122 is 10.2%. This finding is consistent with the outcomes of Shrestha and Subedi (2014) and Singh et al. (2011), but in contrast with the results from Fama and French (1989), Dimson et al. (2005) and Ritter (2005). Moreover, it advocates for the statements of Bansal et al. (2016), Mescereau (2020), and Bansal et al. (2019), who argue that global warming lowers stock market returns.

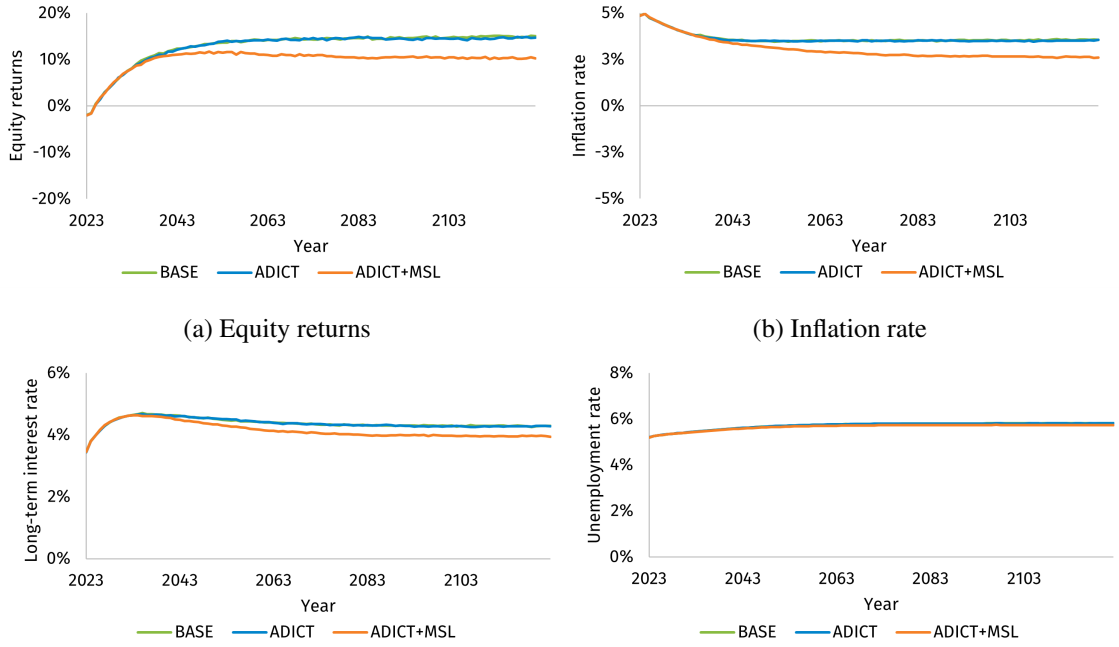


(a) Equity returns

(b) Inflation rate

(c) 10Y-interest rate

(d) Unemployment rate

Figure 6.15: The global economic indicators produced by ADICT+MSL on the RCP2.6 dataset.

Furthermore, in accordance with Friedman (1968), Lim and Sek (2015) and Fuhrer and Olivei (2004), the annual GDP growth rate exhibits a positive relationship with the inflation rate. It drops further to 2.6% due to the additional temperature and mean sea level impact of the CTPs.

Next, regarding the long-term interest rate, ADICT+MSL forecasts a decline of 0.4 percentage points in 2122, compared to BASE. This aligns with the results of Bernanke et al. (2005), Dotsey (2012), and Weitzman (2007) who state that a lower GDP growth rate produces less inflation. Hence, central banks can lower their interest rates.

In contrast with the other variables, the predicted unemployment rate is minimally affected by the global warming. The difference between BASE and ADICT+MSL is negligible, which questions the validity of Okun's law in this research.

Next, analyzing the more realistic future RCP4.5 dataset, similar trends are observed, but at lower

levels and with steeper slopes. In terms of stock returns, BASE projects returns of 10.9% in 2122, while ADICT+MSL forecasts 5.7%, corresponding with 4.2 and 4.5 percentage points differences compared to RCP2.6, respectively. Additionally, the inflation rate declines from 3.6% to 2.7% for BASE and 2.6% to 1.7% with ADICT+MSL. The difference with respect to the long-term interest rate is 0.3% for both models. These significant dissimilarities between RCP2.6 and RCP4.5 illustrate the essence of reduced carbon dioxide emissions. Moreover, the distinct graphs of ADICT+MSL and BASE highlight the crucial inclusion of CTPs in future climate and economic modeling.

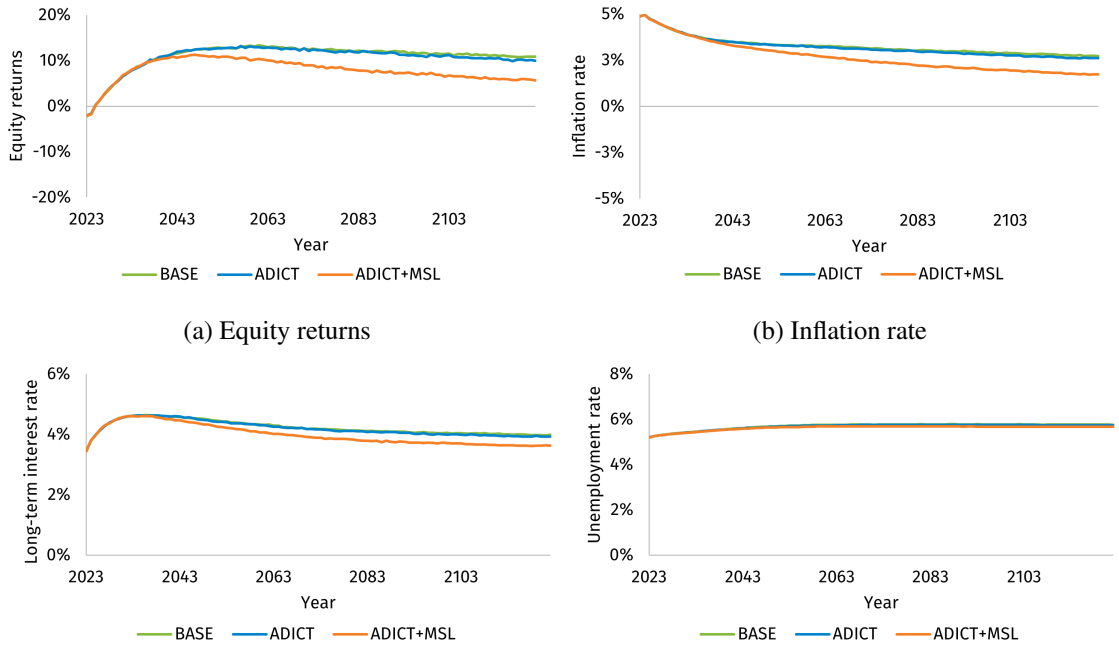


(a) Equity returns

(b) Inflation rate

(c) 10Y-interest rate

(d) Unemployment rate

Figure 6.16: The global economic indicators produced by ADICT+MSL on the RCP4.5 dataset.

Last, the RCP8.5 results represent the worst case scenarios, which could potentially lead to a transformation of humanity as it is presently known. BASE and ADICT+MSL project weighted global equity returns of -1.0% and -12.8% after 100 years of simulation, respectively. Furthermore, the severe temperature trajectories predict stagflation from 2106 for ADICT+MSL. The annual weighted world inflation is estimated at -1.8% with ADICT+MSL. Simultaneously, the 10-year interest rate follows the declining pattern of the inflation and ends at 3.1% for BASE, compared to 4.0% with the RCP4.5 data. Again, the unemployment rate remains relatively unaffected.

In conclusion, global warming, particularly in the ADICT+MSL model, leads to significantly negative equity returns. Moreover, inflation and long-term interest rates decline due to reduced global GDP growth. Contrarily, the unemployment rate exhibits minimal dependence on other economic indicators. These results are consistent across all models for each of the emission trajectories.

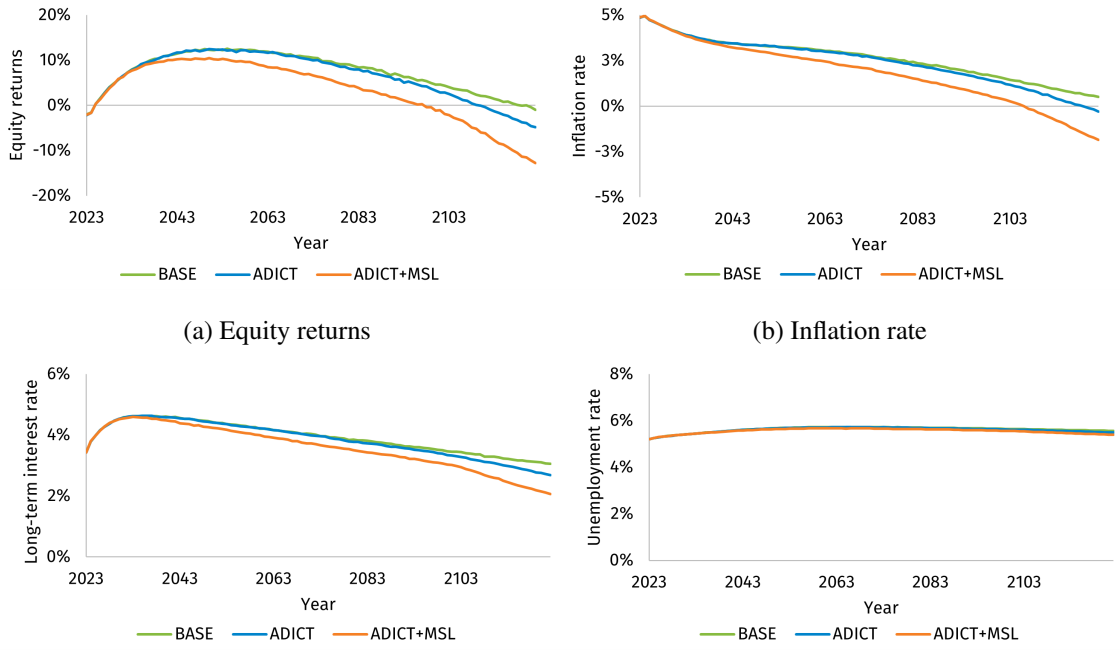


(a) Equity returns

(b) Inflation rate

(c) 10Y-interest rate

(d) Unemployment rate

Figure 6.17: The global economic indicators produced by ADICT+MSL on the RCP8.5 dataset.

### 6.5.2 Short-term shocks

Economic variables are anticipated to experience short-term shocks due to state changes in the CTPs, such as price spikes due to crop failures. Therefore, Figure 6.18 zooms in on a random scenario during the aggregate tipping of GIS, PFAT, and WAIS in 2030. The only time series that is affected by the sudden additional increase in temperature and mean sea level is the stock graph. The annual returns drop from 12.6% to -3.2% within one year. Afterwards they recover again to 12.7%. This indicates the sensitivity of the equity returns to sudden climate shocks. On the other hand, the inflation, long-term interest rates, and unemployment rate show less movement over time due to lower historical standard deviations and the coefficient of the lagged previous observation closer to one, decreasing the dependence on sudden external disturbances.

### 6.5.3 Regional

The regional outcomes of ADICT+MSL are visually presented in world maps for three simulation years, depicted in Figures 6.19-6.22. The maps illustrate the initial values, statistics after 50 years of simulation, and the final values at the end of the 100-year simulation period. Similar to the weighted world maps of GDP growth rates, individual countries exhibit a directional pattern over time. If a financial shows higher values after 50 years, it is expected to increase further. However, unlike the decreasing trend observed in the GDP graphs, the outcomes vary per region.

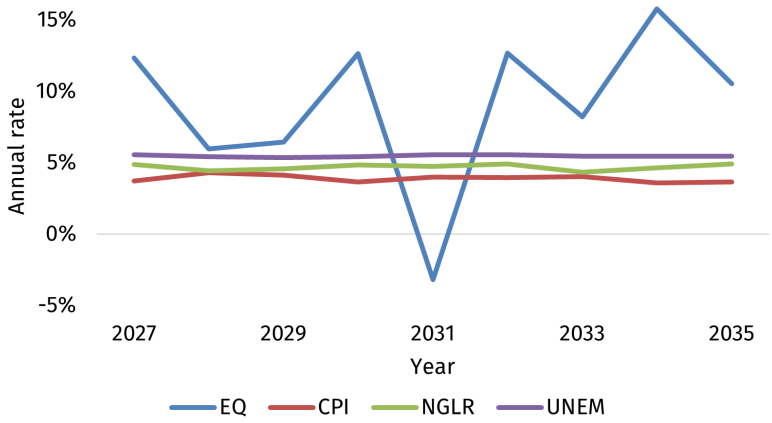


Figure 6.18: Short-term shock of regime shifts in a selection of CTPs.

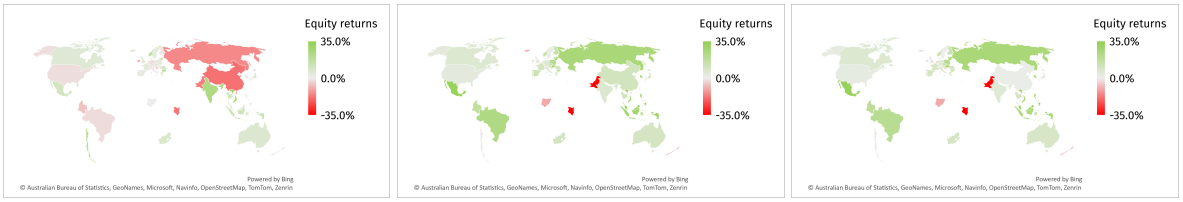


(a) 2023 (b) 2073 (c) 2122

Figure 6.19: World map of equity returns with ADICT+MSL employed on RCP4.5.

Starting with stock returns, initially, 18 regions exhibit negative returns due to the current economic outlook. Croatia, Kenya, and Pakistan are located in the lower regions with predicted returns of -13.6%, -18.3%, -17.7%, respectively. However, also in 2122, these countries experience annual equity losses of more than -10%. Also, in more developed regions, the impact is evident. For instance, in 2122, the Netherlands present returns of -7.5%, New Zealand -4.3%, and The United Kingdom -1.3%. These are drops from the initial values in 2023 of 1.8, 5.1, 7.8 percentage points, respectively. In total, 8 countries depict negative expected annual stock returns in 2122.

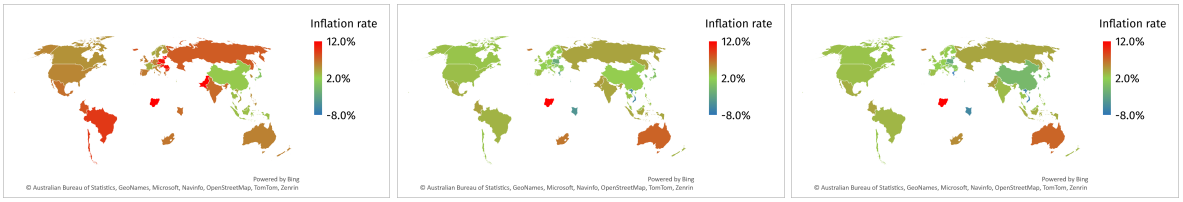


(a) 2023 (b) 2073 (c) 2122

Figure 6.20: World map of inflation rates with ADICT+MSL employed on RCP4.5.

Second, regarding inflation rates, shown in Figure 6.20, the outcomes are more stable due to less deviation in historical inflation rates. Due to the COVID virus, energy crisis, and Russian invasion in Ukraine, the initial price level is above the historical means for the majority of the countries. In

2023, 8 countries report inflation rates above 10%. The relative price levels drop slightly across the simulation horizon, also stimulated by the lower GDP growth rates. For some regions the decrease is substantial. For example, Greece exhibits a drop from 6.7% in 2023 to -9.2% in 2122 and Poland from 11.4% to -2.4% for both simulation years, respectively. Moreover, in 2122, 13 regions present stagflation, with some countries exceeding -5%. The average global inflation decreases from 6.7% to 1.6%, below the targets of most central banks.

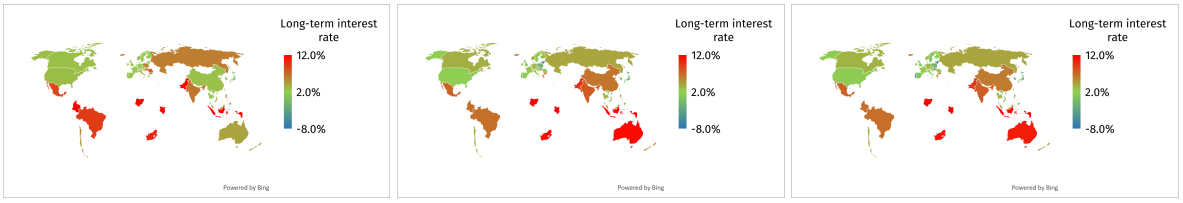


(a) 2023 (b) 2073 (c) 2122

Figure 6.21: World map of 10Y-interest rates with ADICT+MSL employed on RCP4.5.

In line with the overall pattern in forecasted inflation rates, long-term interest rates display similar behavior, projected in Figure 6.21. However, the decrease is less steep. The current long-term interest rates are inflated due to the extreme price levels. For instance, in 2023, Colombia, Indonesia, and Pakistan exhibit interest rates of 12.2%, 18.8%, and 13.5%, respectively. The drop in interest rate is significant for a couple of regions. For example, Lithuania, Portugal and Slovakia, reach interest rates of -14.0%, -5.8%, and -7.0%, far below the world average of 3.4%.

Additionally, another remarking result is evident in the world maps. There are considerable regional correlations, resulting in geographical areas in the map illustrating the same color. In Central America, Africa, and Southern Asia the 10-year interest rate is projected to attain significant high values, while in Northern America, Europe, and Oceania the opposite holds.

Finally, concerning unemployment rates, as mentioned in Section 6.5.1, they are not dependent on global warming. Consequently, throughout time, the time series remain approximately similar. The average absolute difference between 2122 and 2023 is 0.1%. The outliers are the increase of 2.8 percentage points for Brazil, 3.6 for Germany, and 7.8 for Poland. On the other hand, the absolute difference for Mexico, Russia, and the United States is 0.1%.

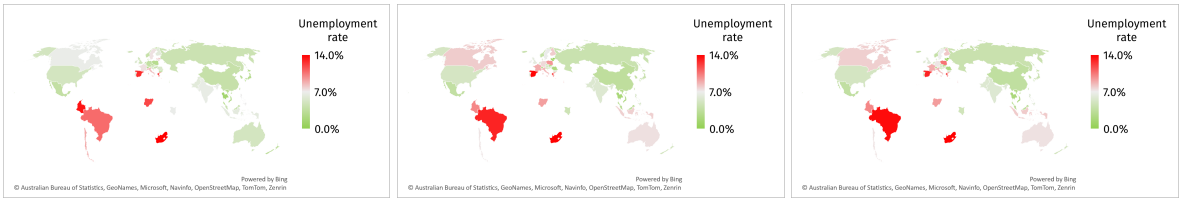


(a) 2023 (b) 2073 (c) 2122

Figure 6.22: World map of unemployment rates with ADICT+MSL employed on RCP4.5.

# Chapter 7

# Discussion

This study includes limitations that should be acknowledged. Firstly, due to the absence of available historical data on recent state changes in CTPs, the model cannot be tested. The introduced ADICT+MSL system is a combination of existing literature findings and intuitive assumptions, such as a logistic activation function and the interaction matrix. However, the outcomes cannot be definitively ascertained because the future remains unsure and no significant global climate mechanisms have undergone destruction in the close past on which the model performance can be examined.

Furthermore, no external negative CTP effects are included, e.g. loss of biodiversity and ecosystems. This omission is intentional to maintain the simplicity and interpretability of the system to maintain the relevance to policy makers. Incorporating additional external damages requires quantifying them and a logical approach of implementing. This would significantly increase the complexity of the model, which is not the objective.

Similarly, for consistency, new technological advancements are excluded as well. Quantifying technological innovations and estimating its impact on individual CTPs requires a significant amount of expert knowledge and creativity, which complicates the ADICT+MSL network.

Moreover, because only the temperature and mean sea level impacts are estimated, CTPs that, according to McKay et al. (2022), decrease temperature, are omitted. Although this approach may introduce a perceived bias towards the global damage of CTPs, including a CTP with a negative effect on temperature leads to positive GDP growth, which is counter-intuitive and not realistic. These other climate mechanisms produce other catastrophic events and are certainly not beneficial to the world.

Last, the results are sensitive to the parameter value for $\tau$, representing the probability of bifurcations. If $\tau$ is set to 0.1, the bifurcations in each of the CTPs happens at a very early stage, also increasing the chance of other CTPs via their interaction and the temperature rise. On the other hand, a value of 0.9 would lead to minimal regime shifting. Therefore, further analysis is necessary to determine an optimal and realistic value for this parameter.

# Chapter 8

# Conclusion

In this study, the ADICT+MSL model is employed on historical climate data to predict the impact of CTPs via global warming on world and regional growth over a simulation horizon of 100 years for different temperature tracks. Additional attention is payed to the indirect effect on financial indicators.

First of all, focusing on the first two sub-questions of this paper regarding the impact of different temperature tracks and mean sea levels, the following is observed. Even without the inclusion of any CTPs, the BASE model decreases the annual global GDP growth rate significantly. The initial weighted GDP growth in 2023 is 3.6%, which declines to 3.3%, 2.4%, and -0.4% in 2122 for the RCP2.6, RCP4.5, and RCP8.5, respectively. Moreover, the downside risk is substantially larger than positive outliers. This indicates the relative damage of more severe temperature tracks.

Additionally, the extra damage due to massive ice sheet CTPs that increase the global mean sea level is concerning. Whereas there is no significant difference between BASE and ADICT, ADICT+MSL produces considerable worse outcomes due to the additional increase in world ocean levels. ADICT+MSL demonstrates annual GDP growth rates of 2.4%, 1.4%, and -3.4%, for the RCP2.6, RCP4.5, and RCP8.5, respectively, corresponding to a decline of 0.9, 1.0, and 3.0 percentage points, compared to BASE. Hence, mean sea level significantly deteriorates the global GDP growth rate.

Next, with respect to the other two sub-questions that examine the relative impact of a higher tipping probability and a larger cascading effect, the results are opposite. The impact of a lower tipping threshold is significant, resulting in a substantially lower GDP growth. For example, a threshold of 0.05 leads to an annual GDP growth for the RCP4.5 data of 1.5%, while this decreases to 1.0% for a threshold of 0.95. On the other hand, varying the interaction among CTPs does not lead to considerable different outcomes.

Apart from the answers to the research questions, the following results are produced that help answer the main research question. Looking at the long-term global cumulative GDP, the difference

between the RCP trajectories is significant. ADICT+MSL produces a cumulative GDP of 1305.7% for RCP2.6, 789.8% for RCP4.5, and 211.9% for RCP8.5. Therefore, it should be prioritized to limit global warming as much as possible.

Furthermore, the GDP growth deteriorates the most in less developed countries. It is evident from the provided world maps that the projected regional GDP growth rates are the lowest in Southern America, Africa, and Southern Asia. This outcome is partially determined by the significantly higher regional temperatures in these countries, but this does not change the fact that these countries are predicted to be impacted the hardest. This is a serious issue because these countries are the least able to defend themselves to extreme losses as a result of higher country debts and less political stability, leading to population migrations to the more developed cooler regions. With the current immigration problems, one can imagine the consequences of such actions.

Regarding the financial indicators, the results differ per asset and on regional level as well. With respect to short-term shocks, only the equity returns series seem to response to regime shifts in CTPs on an annual basis. For the other financial variables, the effect occurs more gradually over time.

To define the impact on the individual economic series, this is a brief summary of the effects. First of all, the annual global weighted equity return with ADICT+MSL is 5.7% for RCP4.5, compared to 10.2% with the RCP2.6 data. On the other hand, the RCP8.5 produces negative returns, indicating the dependency of the stock market on GDP and global warming. A considerable amount of regions expect yearly stock losses with the current anticipated RCP4.5 trajectory, which is a dangerous outcome. Next, inflation rates are projected to balance after the current inflated levels and decline afterwards, demonstrating their positive relation with GDP growth. The RCP8.5 emission trajectory predicts global stagflation from 2106 for ADICT+MSL. Furthermore, the long-term interest rate follows the pattern of the inflation rate and also reduces over time. Interesting to observe is the significant regional correlation. Finally, the unemployment rate is not affected by different climate situations.

In conclusion, higher carbon dioxide emissions provoke global warming, which decreases the projections of the GDP growth. This result is amplified by the rise in mean sea level of certain CTPs. Via the rise in ocean levels, the impact of climate change on the long-term cumulative GDP is terrifying. Moreover, the regional analysis demonstrates the relatively higher impact on warmer less developed countries, which is dangerous. In terms of economic variables, significant negative patterns are derived, affecting the world population directly. Therefore, the researchers of this paper are an advocate of more political and corporate actions, and responsibility for current climate trajectories.

# References


Alley, R., Clark, P., Huybrechts, P., & Joughin, I. (2005). Ice-sheet and Sea-level Changes. *Science*, *310*(5747), 456-460.

Aschwanden, A., Fahnestock, M., Truffer, M., Brinkerhoff, D., Hock, R., Khroulev, C., ... Khan, A. (2019). Contribution of the Greenland Ice Sheet to Sea level over the Next Millennium. *Science Advances*, *5*(6), 1-11.

Ayres, R., & Walter, J. (1991). The Greenhouse Effect: Damages, Costs and Abatement. *Environmental and Resource Economics*, *1*, 237–270.

Babiker, M., & Eckaus, R. (2007). Unemployment Effects of Climate Policy. *Environmental Science and Policy*, *10*(7), 600-609.

Bansal, R., Kiku, D., & Ochoa, M. (2016). Climate Change and Growth Risks. *NBER Working Paper Series*, *23009*, 1-37.

Bansal, R., Kiku, D., & Ochoa, M. (2019). Climate Change Risk. *Federal Reserve Bank of Boston*, 235-239.

Benoit, C. (1924). Note sur une Methode de Resolution des Equations Normales Provenant de l'Application de la Methode des Moindres Carres a un Systeme d'Equations Lineaires en Nombre Inferieur a Celui des Inconnues (Procede du Commandant Cholesky). *Bulletin Geodesique*, *2*, 66-67.

Bernanke, B., Boivin, J., & Eliasz, P. (2005). Measuring the Effects of Monetary Policy: A Factor-Augmented Vector Autoregressive (FAVAR) Approach Get access Arrow. *The Quarterly Journal of Economics*, *120*(1), 387-422.

Biggs, R., Peterson, D., & Rocha, J. (2015). *The Regime Shifts Database: A Framework for Analyzing Regime Shifts in Social-Ecological Systems.* Retrieved from https://www.regimeshifts.org/

Brammer, R., Lightwoord, M., & Rossi, C. (2022). Quantifying the Financial Impacts of Climate Change. A Unified Approach to Physical and Transition Risk. *Conning risk solutions*, *1*, 1-15.

Breusch, T. (1978). Testing for Autocorrelation in Dynamic Linear Models. *Australian Economic Papers*, *17*(31), 334-355.

Breusch, T., & Pagan, A. (1979). A Simple Test for Heteroskedasticity and Random Coefficient Variation. *Econometrica*, *47*(5), 1287-1294.

Brouillette, D. (2023). *From Meteorology to Mitigation: Understanding Global Warming*. Department of Meteorology and Atmospheric Science.

Bulthuis, K., Arnst, M., Sun, S., & Pattyn, F. (2019). Uncertainty Quantification of the Multi-centennial Response of the Antarctic Ice Sheet to Climate Change. *The Cryosphere*, *13*(4), 1349-1380.

Burke, M., & Tanutama, V. (2019). Climatic Constraints on Aggregate Economic Output. *NBER Working Paper*, 1-41.

Bury, T., Sujith, R., Pavithran, I., Scheffer, M., Lenton, T., Anand, M., & Bauch, C. (2021). Deep Learning for Early Warning Signals of Tipping Points. *Applied Mathematics*, *118*(39), 1-9.

Carrington, D. (2022a, August 29). Major Sea-level Rise caused by Melting of Greenland Ice Cap is 'Now Inevitable'. *Guardian*. Retrieved from https://www.theguardian.com/environment/2022/aug/29/major-sea-level-rise-caused-by-melting-of-greenland-ice-cap-is-now-inevitable-27cm-climate

Carrington, D. (2022b, September 8). World on Brink of Five 'Disastrous' Climate Tipping Points, Study Finds. *The Guardian*. Retrieved from https://www.theguardian.com/environment/2022/sep/08/world-on-brink-five-climate-tipping-points-study-finds

Church, J., & White, N. (2013). Sea-level Rise from the Late 19th to the Early 21st Century. *Surveys in Geophysics*, *32*, 582-602.

Cline, W. (1992). The Economics of Global Warming. *Institute for International Economics*, 307-310.

DeConto, R., & Pollard, D. (2016). Contribution of Antarctica to Past and Future Sea-level Rise. *Nature*, *531*, 591-597.

Dietz, S., Rising, J., Stoerk, T., & Wagner, G. (2021). Economic Impacts of Tipping Points in the Climate System. In *National academy of sciences (pnas 2021)* (Vol. 118, p. 1-9). PNAS.

Dimson, E., Marsh, P., & Staunton, M. (2005). Global Evidence on the Equity Risk Premium. *Journal of Applied Corporate Finance*, *15*(4), 27-38.

Dotsey, M. (2012). The Predictive Content of the Interest Rate Term Spread for Future Economic Growth. *FRB Richmond Economic Quarterly*, *84*(3), 31-51.

Dowlatabadi, H. (1995). Integrated Assessment Models of Climate Change: An Incomplete Overview. *Energy Policy*, *23*(4), 289-296.

Durbin, J., & Watson, G. (1971). Testing for Serial Correlation in Least Squares Regression.

*Biometrika*, *58*(1), 1-19.

Fama, E., & French, K. (1989). Business Conditions and Expected Returns on Stocks and Bonds. *Journal of Financial Economics*, *25*(1), 23-49.

Farinotti, D., Huss, M., Furst, J., Landmann, J., Machguth, H., Maussion, F., & Pandit, A. (2019). A Consensus Estimate for the Ice Thickness Distribution of All Glaciers on Earth. *Nature Geoscience*, *12*(3), 168-173.

Farsio, F., & Quade, S. (2003). An Empirical Analysis of the Relationship Between GDP and Unemployment. *Humanomics*, *19*(3), 1-6.

Ferre, J. (2009). *Comprehensive Chemometrics*. Elsevier.

Foster, P., & Shine, K. (2002). Assessing the Climate Impact of Trends in Stratospheric Water Vapor. *Geophysical Research Letters*, *29*(6), 100-104.

Fretwell, P., Pritchard, H., Vaughan, D., Bamber, J., Barrand, N., Bell, R., ... Zirizzotti, A. (2013). Bedmap2: Improved Ice Bed, Surface, and Thickness Datasets for Antarctica. *The Cryosphere*, *7*(1), 375-393.

Friedman, M. (1968). The Role of Monetary Policy. *The American Economic Review*, *58*(1), 1-17.

Fuhrer, J., & Olivei, G. (2004). Estimating Forward-Looking Euler Equations with GMM Estimators: An Optimal Instruments Approach. *Federal Reserve Bank of Boston*, *4*(2), 1-33.

Fung, I., Doney, S., Lindsay, K., & John, J. (2005). Evolution of Carbon Sinks in a Changing Climate. *Environmental Sciences*, *102*(32), 11201-11206.

Godfrey, L. (1978). Testing Against General Autoregressive and Moving Average Error Models when the Regressors Include Lagged Dependent Variables. *Econometrica*, *46*(6), 1293-1301.

Hanes, S. (2022, January 24). Ice shelf collapse: 'Unknown' Antarctica still holds surprises. *ASOC*. Retrieved from https://www.asoc.org/ice-archives/?category=in-the-news

Hansen, J., & et al. (2005). Earth's Energy Imbalance: Confirmation and Implications. *Science*, *308*(5727), 1431-1435.

Harris, I., Osborn, T., Jones, P., & Lister, D. (2020). Version 4 of the CRU TS monthly High-Resolution Gridded Multivariate Climate Dataset. *Scientific Data*, *7*(109), 1-20.

Harvey, C. (2019, April 9). Mountain Glaciers Are Major Contributors to Rising Seas. *Scientific American*. Retrieved from https://www.scientificamerican.com/article/mountain-glaciers-are-major-contributors-to-rising-seas/

Harville, D. (1976). Extension of the Gauss-Markov Theorem to Include the Estimation of Random Effects. *The Annals of Statistics*, *4*(2), 384-395.

Herr, A., Osaka, S., & Stone, M. (2019, July 2). Points of No Return. *Grist*. Retrieved

from https://grist.org/climate-tipping-points-amazon-greenland-boreal-forest/

Hersher, R., & Sommer, L. (2022, November 10). Here are 3 Dangerous Climate Tipping Points the World is on Track for. *npr*. Retrieved from https://www.npr.org/2022/11/10/1133090748/here-are-3-dangerous-climate-tipping-points-the-world-is-on-track-for

Hodrick, R., & Prescott, E. (1997). Postwar U.S. Business Cycles: An Empirical Investigation. *Journal of Money, Credit and Banking*, *29*(1), 1-16.

Hope, C., Anderson, J., & Wenman, P. (1993). Policy Analysis of the Greenhouse Effect: An Application of the PAGE Model. *Energy Policy*, *21*(3), 327-338.

Igini, M. (2022, October 19). The Tipping Points of Climate Change: How Will Our World Change? *EARTH.ORG*. Retrieved from https://earth.org/tipping-points-of-climate-change/

IMF. (2022). *World Economic Outlook*. Retrieved from https://www.imf.org/external/datamapper/datasets/WEO

IPCC. (2014). *Climate Change 2014*. Author.

IPCC. (2022). *Climate Change 2022*. Author.

Jarque, C., & Bera, A. (1980). Efficient Tests for Normality, Homoskedasticity, and Serial Independence of Regression Residuals. *Economics Letters*, *6*(5), 255-259.

J. Hansen, D., Johnson, Lacis, A., Lebedeff, S., Lee, P., Rind, D., & Russell, D. (1981). Climate Impact of Increasing Atmospheric Carbon Dioxide. *Science*, *213*(4511), 957-966.

Johansen, S. (1992). Cointegration in Partial Systems and the Efficiency of Single-equation Analysis. *Journal of Econometrics*, *52*(3), 389-402.

Kahn, M., Mohaddes, K., Ng, R., Pesaran, M., Raissi, M., & Yang, J. (2021). Long-term Macroeconomic Effects of Climate Change: A Cross-Country Analysis. *Energy Economics*, *104*, 120-131.

Kalkuhl, M., & Wenz, L. (2020). The Impact of Climate Conditions on Economic Production. Evidence from a Global Panel of Regions. *Journal of Environmental Economics and Management*, *103*, 1-20.

Karl, T., & Trenberth, K. (2003). Modern Global Climate Change. *Science*, *302*(5651), 1719-1723.

Keen, S., Lenton, T., Godin, A., Yilmaz, D., Grasselli, M., & Garrett, T. (2021). *Economists' Erroneous Estimates of Damages from Climate Change*.

Kemp, L., Xu, C., Depledge, J., & Lenton, T. (2022). Climate Endgame: Exploring Catastrophic Climate Change Scenarios. *Earth, Atmospheric, and Planetary Sciences*, *119*(34), 1–9.

Kuehn, C. (2013). A Mathematical Framework for Critical Transitions: Normal Forms, Variance and Applications. *Journal of Nonlinear Science*, *23*, 457-510.

Kuznetsov, Y. (2004). *Elements of Applied Bifurcation Theory* (3rd ed., Vol. 112). New York: Springer.

Lade, S., Tavoni, A., Levin, S., & Schluter, M. (2013). Regime Shifts in a social-ecological system. *Theoretical Ecology*, *6*, 359-372.

Lenton, T., Livina, V., Dakos, V., Van Nes, H., & Scheffer, M. (2012). Early Warning of Climate Tipping Points from Critical Slowing down: Comparing Methods to Improve Robustness. *Mathematical, Physical and Engineering Sciences*, *370*(1962), 1185-1203.

Levine, L. (2012). Economic Growth and the Unemployment Rate. *CRS Report for Congress*, 1-7.

Lim, Y., & Sek, S. (2015). An Examination on the Determinants of Inflation. *Journal of Economics, Business, and Management*, *3*(7), 678-682.

Ljung, G., & Box, G. (1971). On a Measure of a Lack of Fit in Time Series Models. *Biometrika*, *65*(2), 297-303.

Lontzek, T., Cai, Y., Judd, K., & Lenton, T. (2015). Stochastic Integrated Assessment of Climate Tipping Points Indicates the Need for Strict Climate Policy. *Nature Climate Change*, *5*, 441-444.

Macrotrends. (2022a). *GDP Growth Rate.* Retrieved from https://www.macrotrends.net/countries/ranking/gdp-gross-domestic-product

Macrotrends. (2022b). *GDP Unemployment Rate.* Retrieved from https://www.macrotrends.net/countries/ranking/unemployment-rate

Marquaridt, D. (1970). Generalized Inverses, Ridge Regression, Biased Linear Estimation, and Nonlinear Estimation. *Technometrics*, *12*(3), 591-612.

Marzeion, B., Kaser, G., Maussion, F., & Champollion, N. (2018). Limited Influence of Climate Change Mitigation on Short-term Glacier Mass Loss. *Climate Change*, *8*, 305-308.

Matthews, H., Gillet, N., & Zickfeld, K. (2009). The Proportionality of Global Warming to Cumulative Carbon Emissions. *Nature*, *459*, 829-832.

May, R., Levin, S., & Sugihara, G. (2008). Ecology for Bankers. *Nature*, *451*, 893-894.

McKay, A., Staal, A., Abrahams, J., Winkelmann, R., Sakschewski, B., Loriani, S., ... Lenton, T. (2022). Exceeding 1.5C Global Warming could Trigger Multiple Climate Tipping Points. *Science*, *377*(6611).

McSharry, P., Smith, L., & Tarassenko, L. (2003). Prediction of Epileptic Seizures: are Nonlinear Methods Relevant. *Nature Medicine*, *9*, 241-242.

Meinshausen, M., Smith, S., Calvin, K., Daniel, J., Kainuma, M., Lamarque, J., ... Van Vuuren,

D. (2011). The RCP greenhouse gas concentrations and their extensions from 1765 to 2300. *Climate Change*, *109*(213), 213-241.

Meredith, S. (2023, January 4). Europe Starts 2023 with Historic Winter Heatwave; Snow Shortage Forces Ski Resorts to Close. *CNBC*. Retrieved from https://www.cnbc.com/2023/01/04/europe-begins-new-year-with-historic-winter-heat-ski-resorts-close.html

Mescereau, B. (2020). Fighting Climate Change as a Global Equity Investor. *Journal of Asset Management*, *21*, 70-83.

Mueller, V., Gray, C., & Hopping, D. (2020). Climate-Induced Migration and Unemployment in Middle-Income Africa. *Global Environmental Change*, *65*, 102-183.

Newburger, E. (2023, January 9). The Earth's Ozone Layer is Slowly Recovering, UN Report Finds. *CNBC*. Retrieved from https://www.cnbc.com/2023/01/09/the-earths-ozone-layer-is-slowly-recovering-un-report-finds-.html

Nordhaus, W. (1991). To Slow or Not to Slow: The Economics of The Greenhouse Effect. *The Economic Journal*, *101*(407), 920-937.

Nordhaus, W. (1992). The 'Dice' Model: Background and Structure of a Dynamic Integrated Climate-Economy Model of the Economics of Global Warming. *Cowles Foundation Discussion Papers*, *1252*, 1-133.

Odongo, M., Misati, R., Kamau, A., & Kisingu, K. (2022). Climate Change and Inflation in Eastern and Southern Africa. *Sustainability*, *14*(22), 1-17.

OECD. (2023a). *Gross Domestic Product (GDP).* Retrieved from https://data.oecd.org/gdp/gross-domestic-product-gdp.htm

OECD. (2023b). *Inflation (CPI).* Retrieved from https://data.oecd.org/price/inflation-cpi.htm

OECD. (2023c). *Long-term Interest Rates.* Retrieved from https://data.oecd.org/interest/long-term-interest-rates.htm

OECD. (2023d). *Unemployment Rate.* Retrieved from https://data.oecd.org/unemp/unemployment-rate.htm

Ortec-Finance. (2023). *Dynamic Scenario Generator Data.* Retrieved from https://www.ortecfinance.com/

Pan, L., Powell, E., Latychev, K., Mitrovica, J., Creveling, J., Gomez, N., ... Clark, P. (2021). Rapid Postglacial Rebound Amplifies Global Sea Level Rise following West Antarctic Sea Ice Sheet Collapse. *Science Advances*, *7*(18), 1-9.

Parson, E., & Fisher-Vanden, K. (1997). Integrated Assessment Models of Global Climate Change.

*Annual Review of Energy and the Environment*, *22*, 589-628.

Pattyn, F., Perichon, L., Durand, G., Favier, L., Gagliardini, O., Hindmarsh, R., ... Wilkens, N. (2017). Grounding-line Migration in Plan-view Marine Ice-sheet Models: Results of the Ice2sea MISMIP3d Intercomparison. *Journal of Glaciology*, *59*(215), 410-422.

Pielke, R. (1998). Rethinking the Role of Adaptation in Climate Policy. *Global Environmental Change*, *8*(2), 159-170.

Rahman, M., & Zhang, Q. (2016). Comparison among Pearson Correlation Coefficient tests. *Far East Journal of Mathematical Sciences*, *99*(2), 237-255.

Ravn, M., & Uhlig, H. (2002). On Adjusting the Hodrick-Prescott Filter for the Frequency of Observations. *The Review of Economics and Statistics*, *84*(2), 371-376.

Rebonato, R., Kainth, D., & Melin, L. (2022). Climate Output at Risk. *The Journal of Portfolio Management*, *48*(10), 46-59.

Rignot, E., & Thomas, R. (2002). Mass Balance of Polar Ice Sheets. *Science*, *297*(5586), 1502-1506.

Rising, J., Tedesco, M., Piontek, F., & Stainforth, D. (2022). The Missing Risks of Climate Change. *Nature*, *610*, 643–651.

Ritter, J. (2005). Economic Growth and Equity Returns. *Pacific-Basin Finance Journal*, *13*(5), 489-503.

Rocha, J., Peterson, G., Bodin, O., & Levin, S. (2018). Cascading Regime Shifts within and across Scales. *Science*, *362*(6421), 1379-1383.

Rohde, R. (2023, January 12). Global Temperature Report for 2022. *Berkeley Earth*. Retrieved from https://berkeleyearth.org/global-temperature-report-for-2022/

Rotmans, J., Hulme, M., & Downing, T. (1994). Climate Change Implications for Europe: An Application of the ESCAPE Model. *Global Environmental Change*, *4*(2), 97-124.

Sakamoto, Y., Ishiguro, M., & Kitagawa, G. (1986). Akaike Information Criterion Statistics. *Journal of the American Statistical Association*, *83*(403), 902-926.

Scheffer, M., Bascompte, J., Brock, W., Brovkin, V., Carpenter, S., Dakos, V., ... Sugihara, G. (2009). Early-warning Signals for Critical Transitions. *Nature*, *461*, 53-59.

Schwanitz, V. (2013). Evaluating Integrated Assessment Models of Global Climate Change. *Environmental Modelling and Software*, *50*, 120-131.

Shimer, R. (2012). Reassesing the Ins and Outs of Unemployment. *The Review of Economic Studies*, *79*(2), 1069-1094.

Shrestha, P., & Subedi, B. (2014). Determinants of Stock Market Performance in Nepal. *NRB Economic Review*, 26–40.

Singh, T., Mehta, S., & Varsha, M. (2011). Macroeconomic Factors and Stock Returns: Evidence

from Taiwan. *Journal of Economics and International Finance*, *2*(4), 217-227.

Spafford, L., & MacDougall, A. (2020). Quantifying the Probability Distribution Function of the Transient Climate Response to Cumulative CO2 Emissions. *Environmental Research Letters*, *15*(3), 1-12.

Steehouwer, H. (2010). A Frequency Domain Methodology for Time Series Modelling. *Interest Rate Models, Asset Allocation and Quantitative Techniques for Central Banks and Sovereign Wealth Funds*, 280-324.

Trading-Economics. (2023). *Government bonds 10Y.* Retrieved from https://tradingeconomics.com/bonds

Valle, S., Li, W., & Qin, S. (1999). Selection of the Number of Principal Components: The Variance of the Reconstruction Error Criterion with a Comparison to Other Methods. *Industrial and Engineering Chemistry Research*, *38*(11), 4389-4401.

Vermeer, M., & Rahmstorf, S. (2009). Global Seal Level Linked to Global Temperature. In *National academy of sciences (pnas 2009)* (Vol. 106, p. 21527-21532). PNAS.

Walker, G. (1931). On Periodicity in Series of Related Terms. *Proceedings of the Royal Society of London*, *131*, 518-532.

Weitzman, M. (2007). A Review of The Stern Review on the Economics of Climate Change. *Journal of Economic Literature*, *45*(3), 703-724.

Wheeler, T., & Von Braun, J. (2013). Climate Change Impacts on Global Food Security. *Science*, *341*(6145), 508-513.

White, H. (1980). A Heteroskedasticity-Consistent Covariance Matrix Estimator and a Direct Test for Heteroskedasticity. *Econometrica*, *48*(4), 817-838.

Winkelmann, R., Martin, M., Haseloff, M., Albrecht, T., Bueler, E., Khroulev, C., & Levermann, A. (2011). The Potsdam Parallel Ice Sheet Model (PISM-PIK) – Part 1: Model Description. *The Cryosphere*, *5*, 715-726.

World-Bank. (2023). *Global Economic Monitor (GEM).* Retrieved from https://databank.worldbank.org/source/global-economic-monitor-(gem)

Yule, G. (1927). On a Method of Investigating Periodicities in Disturbed Series, with Special Reference to Wolfer's Sunspot Numbers. *Philosophical Transactions of the Royal Society of London*, *226*, 267-298.

Zemp, M., Huss, M., Thibert, E., Eckert, N., McNabb, R., Huber, J., ... Cogley, J. (2019). Global Glacier Mass Changes and their Contributions to Sea-level Rise from 1961 to 2016. *Nature*, *568*, 382-386.

# Chapter 9

# Appendix

## 9.1 Abbreviations

**ADICT**: Activation and Damage of Interactive Climate Tipping Points (model)

**AIC**: Akaike Information Criterion

**AMAZ**: Amazon Rainforest dieback

**AWSI**: Arctic Winter Sea Ice collapse

**BASE**: Base model without climate tipping points

**CTP**: Climate Tipping Point

**EAIS**: East Antarctic Ice Sheet collapse

**EASB**: East Antarctic Subglacial Basins collapse

**GDP**: Gross Domestic Product

**GIS**: Greenland Ice Sheet collapse

**GLCR**: Mountain Glaciers loss

**IAM**: Integrated Assessment Model

**MSL**: Mean Sea Level (extension)

**PCA**: Principal Component Analysis

**PFAT**: Boreal Permafrost abrupt thaw

**PFTB**: Boreal Permafrost collapse

**TCRE**: Transient Climate Response to cumulative carbon Emissions

**TP**: Tipping Point

**TUND**: Boreal forest Northern Tundra greening

**VAR**: Vector AutoRegressive

**VIF**: Variance Inflation Factor

**WAIS**: West Antarctic Ice Sheet collapse

## 9.2 List of Climate Tipping Points

This section contains a table with the CTPs researched in this study and an additional figure that depicts the geographical locations.

Table 9.1: The list of climate tipping points researched in this study

| CTP | Full name |
|---|---|
| AMAZ | Amazon Rainforest dieback |
| AWSI | Arctic Winter Sea Ice collapse |
| EAIS | East Antarctic Ice Sheet collapse |
| EASB | East Antarctic Subglacial Basins collapse |
| GIS | Greenland Ice Sheet collapse |
| GLCR | Mountain Glaciers loss |
| PFAT | Boreal Permafrost abrupt thaw |
| PFTB | Boreal Permafrost collapse |
| TUND | Boreal forest Northern Tundra greening |
| WAIS | West Antarctic Ice Sheet collapse |

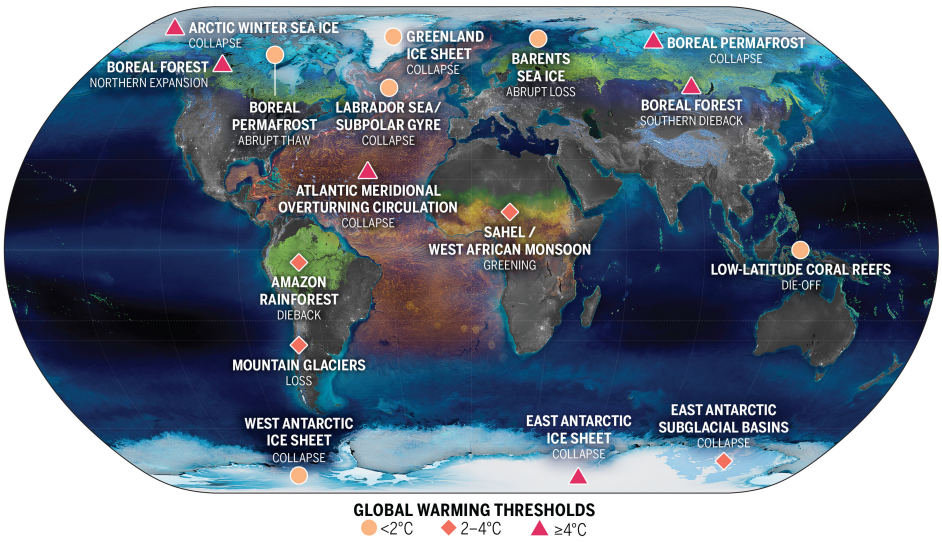


Figure 9.1: A geographical representation of CTPs distributed across the world map. *Adapted from McKay et al. (2022)*

## 9.3 Damage function validity analysis

This section provides an analysis of the damage function outcomes, portrayed in Table 6.1 in Section 6.1. The validity of the *4* linear regression model is examined through various statistical diagnostic residual tests, as described in Section 5.2. These tests include: 1) zero-mean t-test, 2) endogeneity Pearson correlation test, 3) serial correlation Breusch-Godfrey test, 4) heteroskedasticity White test, 5) normality Jarque-Bera test, and 6) VIF examination.

First of all, to examine whether the mean of the residuals equals zero, a Student's t-test is applied with the mean and standard deviation of the residuals. Second, To test for the presence of endogeneity, a Z-test is employed, proposed by Rahman and Zhang (2016): $Z = \frac{\rho}{\sqrt{(1-\rho^2)^2}}\sqrt{T-1} \sim N(0,1)$. If either of the first two tests fails, an alternative model needs to be specified. The zero-mean t-test yields a statistic of 0.00 with a p-value of 1.00, indicating that the residuals possess a mean centered around zero. Furthermore, the Pearson endogeneity correlation test indicates that the correlation between each variable and the residuals falls within the range of $[-0.01, 0.01]$. This proves that the residuals are not correlated with the independent regressors in the damage function, satisfying an important assumption for maintaining the validity of a linear regression.

Next, to assess the level of serial correlation, the Breusch-Godfrey test (Breusch, 1978) (Godfrey, 1978) is employed. It is based on Lagrange Multiplier (LM) testing and has been shown to be more powerful than its competitors, the Durban-Watson test (Durbin & Watson, 1971) and Ljung-Box test (Ljung & Box, 1971). To address the potential issue of serial correlation, Newey-West standard errors are constructed. Furthermore, to investigate the existence of heteroskedasticity, the White test (White, 1980), which is also an LM test, is evaluated. Unlike the Breusch-Pagan test (Breusch & Pagan, 1979), it accounts for non-linear forms of heteroskedasticity. Violation of the homoskedasticity assumption can be resolved by implementing Weighted Least Squares (WLS) or Newey-West standard errors. The Breusch-Godfrey statistic yields a value of 98.8 with a p-value of 0.00, indicating a failure of the test at a 1% significance level. Similarly, the White heteroskedasticity tests yield a White statistic of 183.7, resulting in a p-value of 0.00, suggesting non-constant variance of the residuals. Although ordinary least squares estimation remains unbiased and consistent in the presence of heteroskedasticity and serial correlation in the residuals, it is no longer the efficient estimation method. Considering these characteristics, Newey-West standard errors are an alternative approach to mitigate the adverse effects of serial correlation and heteroskedasticity. This adjustment does not alter the parameter values but adjusts the standard errors. The examination of the residual series includes an assessment of partial autocorrelation to identify and autocorrelations above 0.05. This threshold results in a lag of one for the Newey-West standard errors.

Multicollinearity can be evaluated by examining the Variance Inflation Factor (VIF) introduced by Marquaridt (1970). The VIF statistic provides an estimate of how much of the variance of the regression coefficient is caused by other factors in the regression. It equals one when the selected variable is perfectly orthogonal to all other independent variables in the formula and increases if this is not the case. It is widely recognized that a VIF exceeding 5 for any individual variable indicates the presence of multicollinearity, and regressions should be adjusted if a VIF of more than 10 is observed (Ferre, 2009). In the assessment of multicollinearity between temperature and mean sea level, the VIF statistic is found to be 3.99. This result suggests that there is no need to adjust the exogenous variables in the damage function.

Finally, the normality of the residuals is analyzed using the Jarque-Bera test (Jarque & Bera, 1980). The Jarque-Bera test is rejected at a 1% significance level. However, this assumption is not crucial for linear regression due to the law of large numbers. This mathematical law states that any distribution becomes a normal distribution asymptotically as the number of observations approaches infinity.

## 9.4 Descriptive statistics historical economic data

Table 9.2: Descriptive statistics of the historical data for a subset of the economic series

| Variable | Region | Obs. | Median | Std. Dev. | Min. | Max. | Skew. | Kurt. |
|---|---|---|---|---|---|---|---|---|
| GDP growth rate | United States | 43 | 2.7% | 2.0% | -3.4% | 7.2% | -0.9 | 1.7 |
| | United Kingdom | 43 | 2.4% | 2.7% | -9.3% | 7.4% | -2.0 | 7.4 |
| | Japan | 43 | 1.7% | 2.4% | -5.7% | 6.8% | -0.7 | 1.8 |
| | Germany | 43 | 1.7% | 2.0% | -5.7% | 5.7% | -1.2 | 3.6 |
| | Brazil | 28 | 2.5% | 2.8% | -3.9% | 7.5% | -0.6 | 0.4 |
| | All | 1687 | 3.1% | 3.0% | -14.8% | 24.4% | -1.1 | 3.1 |
| Equity returns | United States | 43 | 11.0% | 13.2% | -24.2% | 34.4% | -0.4 | -0.1 |
| | United Kingdom | 43 | 8.1% | 12.1% | -17.3% | 28.0% | -0.5 | -0.5 |
| | Japan | 43 | 5.4% | 19.0% | -28.5% | 47.9% | 0.1 | -0.5 |
| | Germany | 43 | 5.8% | 18.3% | -24.7% | 40.1% | -0.1 | -0.9 |
| | Brazil | 28 | 3.6% | 46.8% | -56.1% | 128.6% | 0.8 | 0.1 |
| | All | 1687 | 6.5% | 25.0% | -89.9% | 202.9% | 0.5 | 1.0 |
| Inflation rate | United States | 43 | 2.9% | 2.5% | -0.3% | 13.5% | 2.3 | 7.2 |
| | United Kingdom | 43 | 2.6% | 3.2% | 0.0% | 16.8% | 2.3 | 6.4 |
| | Japan | 43 | 0.5% | 1.7% | -1.3% | 7.8% | 1.9 | 5.4 |
| | Germany | 43 | 1.8% | 1.8% | -0.1% | 8.5% | 1.6 | 2.9 |
| | Brazil | 28 | 6.5% | 11.6% | 3.2% | 66.0% | 4.7 | 23.9 |
| | All | 1687 | 2.5% | 3.5% | -4.0% | 85.7% | 1.4 | 3.0 |
| Long-term interest rate | United States | 43 | 5.0% | 3.4% | 0.9% | 13.9% | 0.8 | -0.2 |
| | United Kingdom | 43 | 5.0% | 3.9% | 0.4% | 14.9% | 0.4 | -0.8 |
| | Japan | 43 | 1.7% | 2.6% | -0.1% | 8.7% | 0.8 | -0.7 |
| | Germany | 43 | 4.6% | 2.9% | -0.5% | 10.1% | -0.1 | -1.0 |
| | Brazil | 28 | 7.3% | 4.1% | 4.8% | 23.4% | 2.0 | 5.2 |
| | All | 1687 | 5.0% | 4.0% | -0.5% | 99.8% | 0.6 | 0.8 |
| Unemployment rate | United States | 43 | 5.8% | 1.7% | 3.7% | 9.7% | 0.6 | -0.5 |
| | United Kingdom | 43 | 7.1% | 2.4% | 3.8% | 11.8% | 0.4 | -1.0 |
| | Japan | 43 | 3.1% | 1.0% | 2.0% | 5.4% | 0.5 | -1.1 |
| | Germany | 43 | 7.4% | 2.2% | 2.9% | 11.0% | -0.2 | -1.0 |
| | Brazil | 28 | 11.6% | 2.3% | 6.9% | 14.7% | -0.4 | -0.9 |
| | All | 1687 | 6.5% | 2.2% | 0.2% | 34.6% | 0.5 | 0.0 |

## 9.5 Historical interactions tables

Table 9.3: Domino effects between the climate tipping points

| *Ind./Dep. var.* | | **1** | **2** | **3** | **4** | **5** | **6** | **7** | **8** | **9** | **10** |
|---|---|---|---|---|---|---|---|---|---|---|---|
| 1 | AMAZ | 0 | 0 | 0 | 0 | 0 | 0 | 0 | 0 | 0 | 0 |
| 2 | AWSI | 1 | 0 | 0 | 0 | 0 | 0 | 0 | 0 | 0 | 0 |
| 3 | EAIS | 3 | 0 | 0 | 0 | 0 | 0 | 0 | 0 | 0 | 0 |
| 4 | EASB | 3 | 0 | 0 | 0 | 0 | 0 | 0 | 0 | 0 | 0 |
| 5 | GIS | 4 | 0 | 1 | 1 | 0 | 0 | 0 | 0 | 0 | 1 |
| 6 | GLCR | 1 | 0 | 0 | 0 | 0 | 0 | 0 | 0 | 0 | 0 |
| 7 | PFAT | 1 | 0 | 0 | 0 | 0 | 0 | 0 | 0 | 0 | 0 |
| 8 | PFTB | 1 | 0 | 0 | 0 | 0 | 0 | 0 | 0 | 0 | 0 |
| 9 | TUND | 3 | 1 | 1 | 1 | 0 | 1 | 1 | 1 | 0 | 1 |
| 10 | WAIS | 3 | 0 | 0 | 0 | 0 | 0 | 0 | 0 | 0 | 0 |

Table 9.4: Hidden feedback effects between the climate tipping points

| *Ind./Dep. var.* | | **1** | **2** | **3** | **4** | **5** | **6** | **7** | **8** | **9** | **10** |
|---|---|---|---|---|---|---|---|---|---|---|---|
| 1 | AMAZ | 0 | 0 | 0 | 0 | 5 | 0 | 0 | 0 | 2 | 0 |
| 2 | AWSI | 0 | 0 | 7 | 7 | 0 | 0 | 9 | 9 | 5 | 7 |
| 3 | EAIS | 0 | 7 | 0 | 0 | 24 | 7 | 0 | 0 | 0 | 0 |
| 4 | EASB | 0 | 7 | 0 | 0 | 24 | 7 | 0 | 0 | 0 | 0 |
| 5 | GIS | 5 | 0 | 24 | 24 | 0 | 0 | 10 | 10 | 6 | 24 |
| 6 | GLCR | 0 | 0 | 7 | 7 | 0 | 0 | 9 | 9 | 5 | 7 |
| 7 | PFAT | 0 | 9 | 0 | 0 | 10 | 9 | 0 | 0 | 4 | 0 |
| 8 | PFTB | 0 | 9 | 0 | 0 | 10 | 9 | 0 | 0 | 4 | 0 |
| 9 | TUND | 2 | 5 | 0 | 0 | 6 | 5 | 4 | 4 | 0 | 0 |
| 10 | WAIS | 0 | 7 | 0 | 0 | 24 | 7 | 0 | 0 | 0 | 0 |

The final interaction matrix, denoted as $R$, is presented in Table 9.5. The table displays some interesting findings. First of all, the maximum interaction value between two CTPs is 0.50, for GIS interacting with EAIS, EASB, and WAIS. Furthermore, GIS affects the activation of every other CTP with a minimum connection value of 0.24. This result is not surprising, considering that the melting of Greenland Ice Sheet has far-reaching consequences, leading to significant additions of sea water, temperature changes, and disruptions in global thermohaline circulations. As a result, it triggers catastrophic events such as typhoons, blizzards, and droughts. In contrast, the extinction of the AMAZ only impacts TUND and GIS, making it the CTP with the least cascading effects.

Table 9.5: Interaction matrix of the different climate tipping points.

| *Ind./Dep.* | | **1** | **2** | **3** | **4** | **5** | **6** | **7** | **8** | **9** | **10** |
|---|---|---|---|---|---|---|---|---|---|---|---|
| 1 | AMAZ | 1.00 | 0.00 | 0.00 | 0.00 | 0.22 | 0.00 | 0.00 | 0.00 | 0.14 | 0.00 |
| 2 | AWSI | 0.10 | 1.00 | 0.26 | 0.26 | 0.00 | 0.00 | 0.30 | 0.30 | 0.22 | 0.26 |
| 3 | EAIS | 0.17 | 0.26 | 1.00 | 0.00 | 0.49 | 0.26 | 0.00 | 0.00 | 0.00 | 0.00 |
| 4 | EASB | 0.17 | 0.26 | 0.00 | 1.00 | 0.49 | 0.26 | 0.00 | 0.00 | 0.00 | 0.00 |
| 5 | GIS | 0.30 | 0.00 | 0.50 | 0.50 | 1.00 | 0.00 | 0.32 | 0.32 | 0.24 | 0.50 |
| 6 | GLCR | 0.10 | 0.00 | 0.26 | 0.26 | 0.00 | 1.00 | 0.30 | 0.30 | 0.22 | 0.26 |
| 7 | PFAT | 0.10 | 0.30 | 0.00 | 0.00 | 0.32 | 0.30 | 1.00 | 0.00 | 0.20 | 0.00 |
| 8 | PFTB | 0.10 | 0.30 | 0.00 | 0.00 | 0.32 | 0.30 | 0.00 | 1.00 | 0.20 | 0.00 |
| 9 | TUND | 0.22 | 0.24 | 0.10 | 0.10 | 0.24 | 0.24 | 0.22 | 0.22 | 1.00 | 0.10 |
| 10 | WAIS | 0.17 | 0.26 | 0.00 | 0.00 | 0.49 | 0.26 | 0.00 | 0.00 | 0.00 | 1.00 |

## 9.6 Methodology algorithm

**Algorithm 1** Algorithm that provides the methods to simulate temperature paths and determine damage function parameters

**Require:** historical regional temperatures, $TA_r(t)$, global mean sea levels, $MSL(t)$, regional GDP growth rates, $gdp_r(t)$, global future greenhouse gas emissions, $CO_2(y)$.

**Ensure:** $s = 0$ and $y = 0$ before every step

$S = 2000,\ Y = 100$

Draw $S$ TCREs from $\sim LN(0.789, 0.24)$

**while** $s < S$ **do**

  **while** $y < Y$ **do**

    Project $TA_{A,n}(y) = CO_2(y)/3.7 * TCRE_n$

    $s \leftarrow s + 1, y \leftarrow y + 1$

  **end while**

**end while**

$gdp_r(t) = \alpha + \beta_1 TA_r(t) + \beta_2 TA_r(t)^2 + \gamma[MSL_A(t) - MSL_A(t-1)] + \phi_r$

**Algorithm 2** Algorithm that provides the methods of ADICT+MSL to estime GDP growth

**Require:** historical regional temperatures, $TA_r(t)$, global mean sea levels, $MSL_A(t)$, global future temperatures, $TA_A(y)$, and interaction values, $c_{i,j,dom}$ and $c_{i,j,hid}$ for climate tipping points $i$ and $j$.

**Ensure:** $i = 0,\ j = 0,\ s = 0$ and $y = 0$ before every step

$N = 10,\ S = 1000,\ Y = 100$

**while** $i < N$ **do**

$\delta_i = 5 - (1 + 0.2 * \upsilon_i) * [(Max.TA_i^* - Min.TA_i^*)/2]$

**while** $j < N$ **do**

$\rho_{i,j} = \frac{1}{w}\sqrt{\frac{\overrightarrow{c_{i,j,dom}}+c_{i,j,hid}}{C_{dom}+C_{hid}}},\ j \leftarrow j + 1$

**end while**

$j = 0,\ i \leftarrow i + 1$

**end while**

**while** $s < S$ **do**

**while** $y < Y$ **do**

**while** $i < N$ **do**

$t^*$ is tipping year, $I_x$ is maximum period, $TA$ or $MSL$ of CTP $i$

$TA_{CTP,i}(y) = \frac{t^*}{I_T} * I_{TA}, A_i(y) \geq \tau\ \cap\ t^* \leq I_T$

$MSL_{CTP,i}(y) = \frac{t^*}{I_T} * I_{MSL}, A_i(y) \geq \tau\ \cap\ t^* \leq I_T$

$i \leftarrow i + 1$

**end while**

$\Delta TA(y) = TA_A(t) + \sum_{i=1}^{N} TA_{CTP,i}$

$TA_r(y) = TA_r(0) + \Delta TA(y)$

$MSL(y) = -0.76 + 0.94\ MSL(y-1) + 0.76\ \Delta TA(y)(y) + 0.70\ \Delta TA(y)(y-20) + \sum_{i=1}^{N} MSL_{CTP,i}(y)$

**while** $i < N$ **do**

$z_i(y) = \omega \sum_{j=1\ j\neq i}^{N} \rho_{j,i} * 1_j$

$A_i(y) = \frac{1}{1+e^{-\delta_i\ [\Delta TA(y)-(TA_i{}^*-\ z_i(y))]}}$

$1_i = A_i(t) \geq \tau, i \leftarrow i + 1$

**end while**

Calculate $gdp_r(y)$ and weighted $gdp(y)$, with damage function and $TA_r(y)$ and $MSL(y)$

$y \leftarrow y + 1$

**end while**

$s \leftarrow s + 1$

**end while**

**Algorithm 3** Algorithm that provides the methods to estimate regional economic series

**Require:** historical global weighted GDP growth rates, $gdp(t)$, economic series, $eco_r(t)$, and future global GDP growth, $gdp(y)$

**Ensure:** $r = 0,\ s = 0$, and $y = 0$ before every step

$R = 216(4 * 54),\ S = 1000$, and $Y = 100$

Split economic series in two domains, $bc$ and $trend$, with Hodrick-Prescott filter:

$\min_\xi(\sum_{t=1}^{T}(y(t) - \xi(t))^2 + \lambda \sum_{t=2}^{T-1}[(\xi(t+1) - \xi(t)) - (\xi(t) - \xi(t-1))]^2)$

Apply PCA on historical economic series, $eco_r(t)$

Replace first factor of historical PCA, $F_d(t)$, with $gdp(t)$ and estimate regression parameters

**while** $r < R$ **do**

$eco_{d,r}(t) = \alpha + \phi_{d,r} eco_{d,r}(t-1) + B_{d,r} F_d(t)$

$r \leftarrow r + 1$

**end while**

Simulate PCA factors with Yule-Walker equations and copula errors from the residual covariance matrix:

**while** $y < Y$ **do**

$\gamma_m = \sum_{k=1}^{p} \iota_k \gamma_{m-k} + {\sigma_\epsilon}^2 \eta_{m,0}$

$C_R^{Gauss}(u) = \Phi_R[\Phi^{-1}(u_1, ..., \Phi^{-1} u_k)]$

$F_d(y) = \beta + A F_d(y-1) + \chi_y(t)$

$y \leftarrow y + 1$

**end while**

Replace first vector of future PCA factors with $gdp(y)$

Simulate economic series with the future PCA factors, the historical regression coefficients, and copula errors from the residual covariance matrix

## 9.7 Example of a scenario path

To enhance the understanding of the model, a practical scenario is provided in Figure 9.2. This graph illustrates the projected temperature and GDP growth rate derived from a randomly selected scenario employing the ADICT+MSL model with the RCP8.5 emission path. The temperature is depicted as the global anomaly relative to the 1850-1900 IPCC mean, while the GDP growth rate represents the outcome of the damage function in Equation 5.5 from Section 5.2. The values of the free parameters, $\tau$ and $\omega$, are set to 0.4 and 1.0, respectively, in line with the methodology employed in the remaining sections of this study. The labels indicate the tipping points for the CTPs.

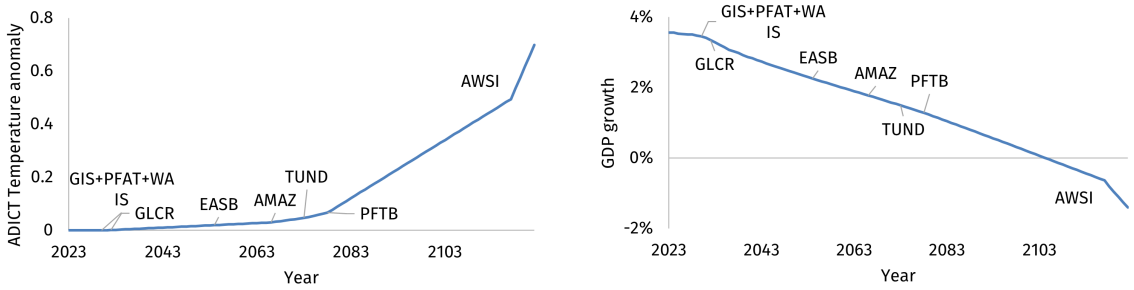


(a) Temperature

(b) GDP growth rate

Figure 9.2: Display of the expected global anomaly temperature and weighted global GDP growth for one random scenario to show the effect of tipping of the CTPs. The scenario is run with the RCP8.5 emission path.

Figure 9.2a highlights significant shifts in the increasing temperature resulting from bifurcations in CTPs. Furthermore, the influence of certain CTPs, such as AWSI and EAIS, is more pronounced compared to others, which can be attributed to their respective temperature impact statistics. This critical temperature, denoted as $I_{TA}$, is 0.6, which is considerable higher compared the other statistics. These numbers as tabulated in Table 4.2 in Section 4.3. Notice that GIS, PFAT, and WAIS exhibit regime shifts simultaneously in the year 2030. This simultaneous occurrence arises from the global temperature surpassing the standard $\tau$ threshold of 0.4, activating their respective activation functions. Since their critical temperature activation values are identical at 1.5 degrees Celsius, the activation of these events concurrently is anticipated. Additionally, these CTPs possess the lowest threshold statistic, denoted as $TA^*$, among all the CTPs, explaining the early instances of bifurcations observed in the simulation path.

Regarding the GDP growth rate depicted in Figure 9.2b, it gradually declines over time due to the adverse influence of higher temperatures and mean sea level, as driven by Equation 5.5. However, the impact of bifurcations in the CTPs is less apparent. Still, in the early years of simulation, a

steeper slope is observed after GIS, PFAT, GLCR, and WAIS have tipped. Also towards the end of the horizon, AWSI significantly evokes a decreasing GDP growth trend. Thus, while the CTPs exert a substantial direct impact on Earth's climate, their direct translation into weighted global GDP growth rates is less definite, but still evident in the model outcomes.

## 9.8 Explanation Python code

The Python code is available through github https://github.com/jorisknoester/ADICT-MSL.

- **generate-config.py**: Writes settings to configuration file.
- **helper.py**: Retrieves the data from the configuration settings.
- **main.py**: Main file that starts the simulation and writes the results to Excel.
- **climate-tipping-point.py**: Class that represents a climate tipping point.
- **eco-monte-carlo-simulation.py**: Computes the future economic series with the use of Monte Carlo simulation, principal components, and copula techniques.
- **environment.py**: The simulation environment that contains the climate tipping points and their effect on GDP with the ADICT model.
- **climate-data.py**: Class that retrieves the climate variable data.
- **climate-tipping-point-data.py**: Class that retrieves the climate tipping point data.
- **country.py**: Class that represents an individual region.
- **get-regression-data.py**: Prepares the regression data from the old raw data to the transformed Excel file. Not required in the simulation, only once to obtain appropriate data format.
- **regression.py**: Performs the regression of the damage function on the historical data.